AD NUMBER

AD916420

NEW LIMITATION CHANGE

TO

Approved for public release, distribution unlimited

FROM

Distribution authorized to U.S. Gov't. agencies only; Test and Evaluation; 24 Jan 1974. Other requests shall be referred to Naval Air Systems Command, Washington, DC.

AUTHORITY

USNASC ltr, 3 May 1974

THE ANALYTIC SCIENCES CORPORATION

(12) 145 p.

(14) TASC-TR-245-1-Vol-1

(6) STUDY OF TACTICAL MISSILE GUIDANCE: ACCURACY LIMITATIONS AND GUIDANCE SENSITIVIES. VOLUME I.

(9) FINAL REPORT.,

(11) 29 Jun 73

DISTRIBUTION LIMITED TO U.S. GOVERNMENT AGENCIES ONLY;
- ☐ FOREIGN INFORMATION
- ☐ PROPRIETARY INFORMATION
- ☒ TEST AND EVALUATION
- ☐ CONTRACTOR PERFORMANCE EVALUATION

DATE: 1-24-74
OTHER REQUESTS FOR THIS DOCUMENT MUST BE REFERRED TO COMMANDER, NAVAL AIR SYSTEMS COMMAND, AIR-5332

Prepared under:
Contract No. (15) N00019-72-C-0392
for
NAVAL AIR SYSTEMS COMMAND
Washington, D. C.

Vol 2 528 6536

Prepared by:
(10) Dale W. Klein
Arthur A. Sutherland, Jr.

Approved by:
Arthur Gelb

THE ANALYTIC SCIENCES CORPORATION
6 Jacob Way
Reading, Massachusetts 01867

404 565

ABSTRACT

This report covers the results of limiting guidance accuracy studies for nine proposed aided inertial guidance techniques. In each case an optimum information handling scheme was assumed. This provides a consistent framework for comparing alternative schemes and determining the desired lower limit on errors for each technique. The report also develops the sensitivities of missile guidance errors to sensor errors and initial alignment errors for three unaided guidance techniques -- inertial guidance and heading command guidance with and without wind compensation. The sensitivity tables provided allow rapid comparisons of different inertial sensors and alignment techniques which may be suggested for use in proposed guidance systems.

TABLE OF CONTENTS

TABLE OF CONTENTS (Continued)

LIST OF FIGURES

LIST OF FIGURES (Continued)

LIST OF TABLES

LIST OF TABLES (Continued)

1. INTRODUCTION

This report concerns a continuing study of various air-to-surface missile guidance techniques. It presents the results of limiting accuracy studies for various inertial guidance techniques. It also presents the sensitivity analysis of missile guidance errors to sensor errors and initial alignment errors for heading command guidance, position reference (inertial) and wind compensated heading command guidance.

1.1 OVERVIEW

Accuracy Limits for Aided Inertial Guidance Techniques — Every new guidance technique, whether based on a new advance in sensor design or a new data blending scheme, has associated with it basic performance limitations. It is important that these limitations be evaluated in each case and that decisions not be based on oversimplified analyses which, for example, treat only the reductions in error contributions which previously limited performance. Calculation of lower bounds on the attainable accuracy of specific guidance techniques requires identification of fundamental error sources and determination of their individual contributions to system error. These calculations may be simplified by assuming that the system under study employs an optimum information handling scheme. This assumption provides a consistent framework against which alternative suboptimal schemes can be compared. It also provides, for each competing guidance technique, the desired lower limit values. This is the viewpoint adapted in the limiting accuracy studies

reported in this document. The limiting accuracies of nine proposed inertial guidance techniques are discussed. These systems cover a wide range of possible system designs. The limiting factors considered can be grouped into the following areas: geometric dilution, propagation uncertainties, geophysical uncertainties, electronic clock accuracy, and other external aid fix errors. The effect of these factors on the guidance techniques were considered and detailed numerical results are presented.

Inertial Guidance Sensitivity Study — Sensitivity studies were performed relating air-to-surface missile guidance errors to sensor errors and initial alignment errors for five representative trajectories. The guidance techniques considered are:

- Heading Command
- Position Reference (Pure Inertial)
- Wind Compensated Heading Command

Results are presented in the form of sensitivity tables which allow the rapid evaluation of guidance errors for particular trajectories, based on inertial sensor errors and alignment errors. These tables are valuable in performing accuracy tradeoff studies of inertial sensors and alignment techniques for use in proposed guidance systems.

1.2 FORMAT OF THE REPORT

Chapter 2 documents the limiting accuracy studies of the aided inertial guidance techniques. The limiting factors are discussed and the results of the analyses of the nine techniques are presented. This chapter

is augmented by Volume II (classified SECRET) of this report, which provides details on satellite/inertial and radar correlation/inertial techniques. Chapter 3 describes the guidance accuracy sensitivity analyses performed. The three guidance techniques and five trajectories considered are described. The sensitivity tables for each of the trajectory/guidance technique combinations are given with sample calculations demonstrating their use. Chapter 4 summarizes the main findings of the work described in this document and relates the value of the analyses to current and future air-to-surface missile guidance problems.

2. ACCURACY LIMITS FOR AIDED INERTIAL GUIDANCE TECHNIQUES

This chapter concerns the calculation of the limiting accuracy for nine proposed inertial guidance techniques for air-to-surface missiles. These accuracy limits provide both a lower bound on the attainable accuracy of the specific guidance techniques and a consistent baseline for comparison of alternative schemes. The factors considered to limit the guidance accuracy were geometric dilution propagation uncertainties, geophysical uncertainties, electronic clock accuracy, and other external aid fix errors. These factors are discussed in detail in the next section. The influence of these factors on the nine inertial techniques listed below is also contained in this chapter.

- Pure Inertial Guidance
- LORAN/Inertial Guidance
- Direct Ranging LORAN/Inertial Guidance
- OMEGA/Inertial Guidance
- DME/Inertial Guidance
- Satellite/Inertial Guidance*
- Radar Correlation/Inertial Guidance*
- Optical Correlation/Inertial Guidance
- Doppler/Inertial Guidance

*Details are presented in the Volume II of this report(Ref. 7).

2.1 FACTORS LIMITING MISSILE GUIDANCE ACCURACY

2.1.1 Geometric Dilution

Many radio navigation systems provide measurements which locate the receiver on a line of position (LOP). The position of the receiver is then determined in two dimensions at the point of crossing of two LOP's. The angle of crossing of these two LOP's greatly influences the radial error in the target location. In the region of crossing the LOP's may be considered straight lines. If each measurement of the LOP has an error ϵ associated with it, the error in the location of the receiver is shown in Fig. 2.1-1. From the figure it can be seen that

$$p = \frac{\epsilon_1}{\sin\theta}$$

$$q = \frac{\epsilon_2}{\sin\theta} \qquad (2.1\text{-}1)$$

From the law of cosines

$$d^2 = p^2 + q^2 + 2pq\cos\theta \qquad (2.1\text{-}2)$$

or

$$d^2 = \frac{1}{\sin^2\theta}\left(\epsilon_1^2 + \epsilon_2^2 + 2\epsilon_1\epsilon_2\cos\theta\right) \qquad (2.1\text{-}3)$$

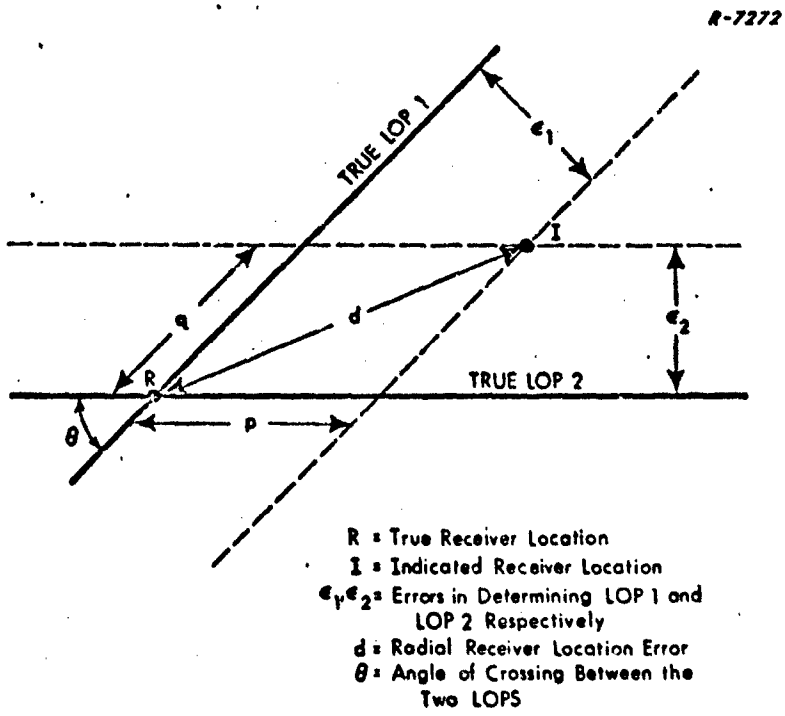

Figure 2.1-1 Effect of LOP Errors on Receiver Location Error

Assuming ϵ_1 and ϵ_2 are zero-mean random variables whose statistics are described by the following quantities:

σ_1 = standard deviation of the error, ϵ_1, in the measurement of LOP 1

σ_2 = standard deviation of the error, ϵ_2, in the measurement of LOP 2

ρ = the correlation coefficient between the measurement errors of LOP 1 and LOP 2

and taking the expected value of the terms in Eq. (2.1-3), the square of the standard deviation of the radial error in receiver location, σ_d^2, is

$$\sigma_d^2 = \frac{1}{\sin^2\theta}\left(\sigma_1^2+\sigma_2^2+2\rho\sigma_1\sigma_2\cos\theta\right) \qquad (2.1\text{-}4)$$

$$\sigma_d = \frac{1}{\sin\theta}\left(\sigma_1^2+\sigma_2^2+2\rho\sigma_1\sigma_2\cos\theta\right)^{1/2} \qquad (2.1\text{-}5)$$

As can be seen from Eq. (2.1-5) the standard deviation of the receiver location error is highly sensitive to the angle between the LOP's. This geometry dependence, which has the effect of always raising σ_d, when $\theta-\pi/2$ is not a multiple of π, is known as geometric dilution.

Two major types of radio navigation systems are considered here. One generates hyperbolic lines of position as in Fig. 2.1-2 by measuring phase or time differences; examples are OMEGA or conventional LORAN systems. It can be shown that the angle of crossing of the LOP's is

$$\theta = \frac{\varphi_1+\varphi_2}{2} \qquad (2.1\text{-}6)$$

for the three-station configuration shown in Fig. 2.1-2. The second type of radio navigation system considered generates circular lines of position, as in Fig. 2.1-3, by providing direct measurement of range to the receiver (one possibility is that the measurement is in the form of time for the signal to arrive from the station, which can be converted to range simply by multiplying the propagation time by the velocity of light) from one station, as with Direct Ranging LORAN (see Ref. 1). For this type of system the angle of crossing of the LOP's is

$$\theta = (\pi - \varphi) \qquad (2.1\text{-}7)$$

where φ is defined in Fig. (2.1-3).

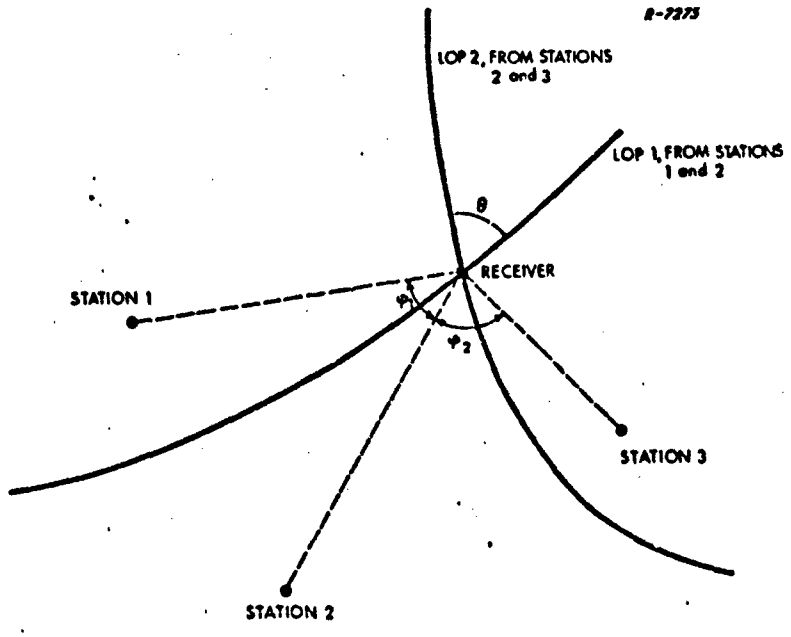

Figure 2.1-2 Three-Station Configuration Illustrating the Crossing Angle of Hyperbolic LOP's

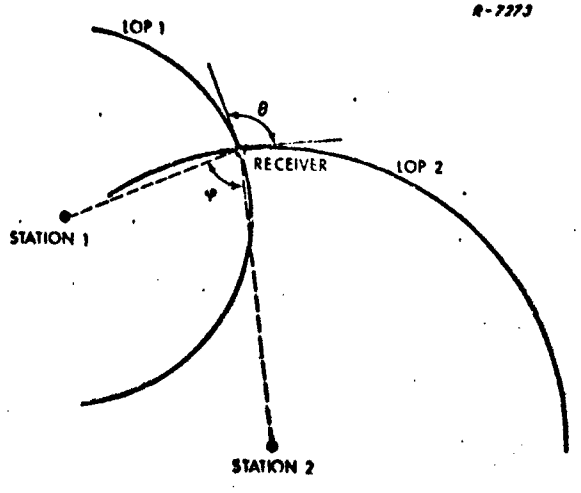

Figure 2.1-3 Two-Station Configuration Illustrating the Crossing Angle of Circular LOP's

By combining Eqs. (2.1-5) and (2.1-6) it can be shown that for a hyperbolic system the standard deviation of the radial error in receiver location, σ_d, is given by

$$\sigma_d = \frac{1}{\sin\left(\frac{\varphi_1+\varphi_2}{2}\right)}\left(\sigma_1^2+\sigma_2^2+2\rho\sigma_1\sigma_2\cos\left(\frac{\varphi_1+\varphi_2}{2}\right)\right)^{1/2} \qquad (2.1\text{-}8)$$

where φ_1 and φ_2 are determined by the fix geometry (Fig. 2.1-2). Combining Eqs. (2.1-5) and (2.1-7) gives the rms radial error for a circular system as

$$\sigma_d = \frac{1}{\sin\varphi}\left(\sigma_1^2+\sigma_2^2-2\rho\sigma_1\sigma_2\cos\varphi\right)^{1/2} \qquad (2.1\text{-}9)$$

where φ is defined by the fix geometry (Fig. 2.1-3).

2.1.2 Propagation Uncertainties

Radio waves can be considered to propagate over the earth in either a ground wave and/or skywave mode. Ground waves propagate by following the curvature of the earth and are generally high frequency waves. This mode of propagation is characteristic of such systems as LORAN. Skywaves propagate by reflecting in a wave guide formed by the ionosphere and the earth's surface. These waves are generally low frequence, characteristic of such systems as OMEGA. The two propagation modes are illustrated in Fig. 2.1-4. Since the ground waves are propagated directly to the receiver the time between

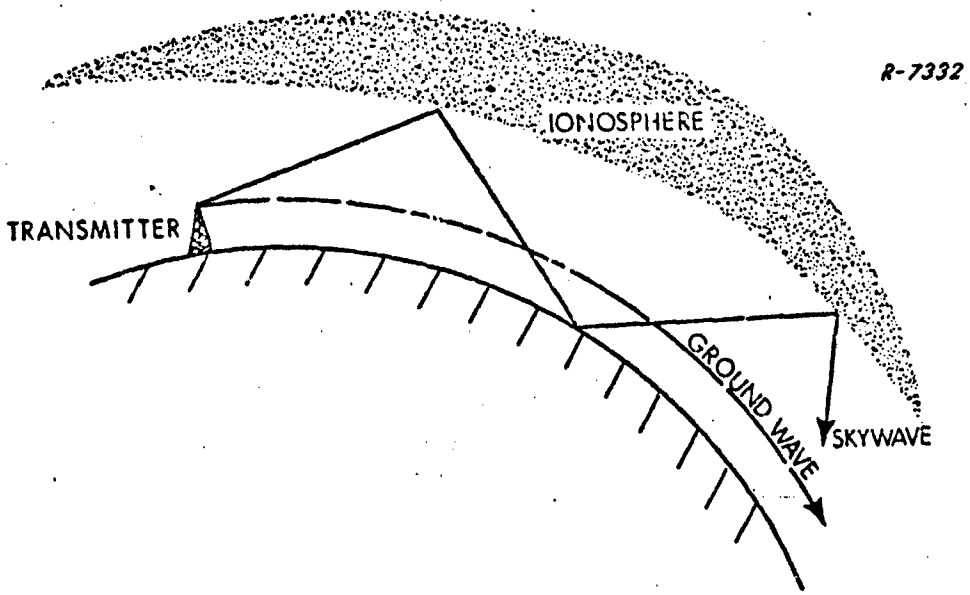

Figure 2.1-4 Illustration of Ground Wave and Skywave Propagation

transmission and reception, T, can be related to the range (ground distance or slant range), R, between the transmitter and receiver by Eq. (2.1-10)

$$T = \frac{R}{c} \qquad (2.1\text{-}10)$$

where c is the velocity of light. The latter is equal to the nominal velocity of light in the atmosphere, c_o, and the variation in the velocity, δc, due to uncertainties in atmospheric conductivity caused by atmospheric disturbances, water vapor concentration, etc. Equation (2.1-10) can be rewritten

$$T = \frac{R}{c_o + \delta c} \qquad (2.1\text{-}11)$$

Since the uncertainty, δc, is small compared to c_o Eq. (2.1-11) can be approximated as

$$T = \frac{R}{c_o}\left(1 - \frac{\delta c}{c_o}\right) \qquad (2.1\text{-}12)$$

The propagation uncertainty or delay due to uncertainties in the speed of light, δT, for ground waves can be separated from the above equation as

$$\delta T = \frac{R\delta c}{c_o^2} \qquad (2.1\text{-}13)$$

The term $\delta c/c_o$ may be considered a random scale factor error, α. The propagation uncertainty for ground waves* can therefore be modeled as a random scale factor times the propagation time of a wave over a similar distance at the nominal velocity of light in the atmosphere, R/c_o

$$\delta T = \frac{R}{c_o}\,\alpha \qquad (2.1\text{-}14)$$

Although a similar range-dependent effect in propagation uncertainty occurs with skywaves its influence is outweighed by random delays due to ionosphere altitude variations and ionospheric disturbances. For skywave propagation, the propagation uncertainties are best modeled

*These equations also apply for other forms of direct transmission such as satellite radio transmissions passing through the atmosphere.

as a random bias error* independent of the range between the transmitter and receiver.

The effect of propagation uncertainties for radio navigation systems is to cause errors in determining the LOP's on which the receiver lies.

2.1.3 Geophysical Uncertainties

Inertial systems operate under the assumption that the earth's gravity field (net result of earth's gravitational attraction and centripetal acceleration experienced from the earth's rotation) has equipotential surfaces which are elliposidal in shape. ** Inertial systems must compensate for the specific force due to gravity using knowledge of the gravity field. However, many deviations from the ideal gravity surface exist, appearing as variations in the direction and magnitude of the gravity vector; the former are referred to as gravity deflections and the latter as gravity anomalies. They result from the fact that the earth is not a smooth homogeneous body. Their effect on the navigator position error can usually be reduced when external position fixes are available.

Gravity anomalies and vertical deflections are typically modeled as first-order markov processes whose correlation times are

---

*This model applies when considering tactical missiles due to the short time of flight. Daily and seasonal variations do occur which alter the model for longer time intervals.

**Even the harmonic equipotential surfaces measured and used in satellite applications do not account for the variations discussed here.

inversely proportional to vehicle velocity. * Vertical deflections are assumed to enter the system in the form of small disturbance inputs to level loop accelerometers. For analysis of inertial systems in tactical missiles, velocity and position errors can be computed on the basis of open-loop propagation of these errors; the tactical missile flight time is short relative to the 84-min. mode of inertial navigator level loops. The vertical deflection disturbances, δ, are assumed to be random, zero mean quantities with autocorrelation function:

$$\varphi_{\delta\delta}(\tau) = \sigma_\delta^2 e^{-\frac{|\tau|}{T_\delta}} \qquad (2.1\text{-}15)$$

Because vertical deflections exhibit a spacial rather than temporal variation, the time constant T_δ is computed from a distance correlation D_δ by assuming constant missile horizontal velocity, V:

$$T_\delta = \frac{D_\delta}{V} \qquad (2.1\text{-}16)$$

The velocity and position errors in each level loop are generated according to

$$e_v = \int_0^t e_\delta(\eta)\, d\eta \qquad e_p = \int_0^t e_v(\eta)\, d\eta \qquad (2.1\text{-}17)$$

*The analysis here is a portion of the work previously discussed in Ref. 2. Also considered in Ref. 3 was a second-order markov model for the vertical deflections and gravity anomalies. The results obtained from the second-order model were very similar to the first-order model, so only one set of analyses is presented in this report.

Mean square values of position and velocity errors are given by

$$\overline{e_v^2} = 2T_\delta \sigma_\delta^2 \left[t - T_\delta \left(1 - e^{-t/T_\delta} \right) \right]$$

$$\overline{e_p^2} = 2T_\delta \sigma_\delta^2 \left[\frac{t^3}{3} - \frac{T_\delta}{2} t^2 - T_\delta^2 t e^{-t/T_\delta} + T_\delta^3 \left(1 - e^{-t/T_\delta} \right) \right] \qquad (2.1\text{-}18)$$

Under the assumption of constant missile velocity, the quantity t/T_δ at the target is the ratio of missile range, R, to D_δ. Defining

$$a = \frac{R}{D_\delta}$$

and dropping the subscript notation, the expressions for mean square errors at the target are:

$$\overline{e_v^2} = 2T\sigma^2 t \left[1 - \frac{1}{a} (1 - e^{-a}) \right]; \qquad t = \frac{R}{V}$$

$$\overline{e_p^2} = 2T\sigma^2 t^3 \left[\frac{1}{3} - \frac{1}{2a} - \frac{1}{a^2} e^{-a} + \frac{1}{a^3} (1 - e^{-a}) \right] \qquad (2.1\text{-}19)$$

Figure A.3-1 illustrates these relations. Since external position fixes can reset position errors in inertially aided systems these errors are generally considered important only for pure inertial navigation.

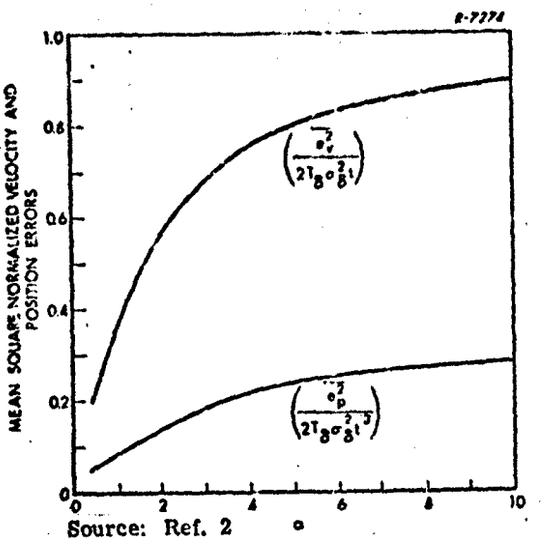

Source: Ref. 2

Figure 2.1-5 Mean Square Normalized Velocity and Position Errors as a Function of the Parameters "a"

2.1.4 Electronic Clock Accuracy

Some radio navigation systems such as Direct Ranging LORAN locate the receiver on a circular LOP by measuring the time required for a signal to travel from a master station. Such systems require the user to have a clock on board to determine the time of signal arrival; information giving the time the signal was sent and the station from which it was sent is contained in the signal. The propagation time is therefore the difference between the time of signal arrival (from the user clock) and the time the signal was sent. This can be converted to range from the transmitting station by multiplying the propagation time by the velocity at which radio signals propagate. In most cases the user clock is a quartz-crystal clock and this will be assumed for the present studies. The accuracy in determining the time of signal arrival effects the error in determining the LOP on which the receiver lies. The error sources encountered in crystal clocks are described below.

Initial Phase Error — This error is the actual time difference between the receiver clock and the reference master station clock before any calibration procedures begin. Since the phase of an unsynchronized crystal oscillator is arbitrary, the initial phase error may be quite large (e.g., 1-10 μsec). The residual error in the initial phase error after synchronization with the master clock contributes to the LOP location error.

Frequency Offset Error — Frequency offset error refers to the difference in frequency between the quartz-crystal clock and the master clock immediately after synchronization has been achieved. These errors are a combination of frequency measurement error and limitations on the adjustability of the quartz-crystal clock frequency. Any initial frequency error will result in a linear phase error build-up with time. This phase error build-up is determined by considering the nominal clock frequency f_o and τ_o, the corresponding period. The frequency fractional error, δ, is given by

$$\delta = \frac{f - f_o}{f_o} = \frac{\Delta f}{f_o} \qquad (2.1\text{-}20)$$

where f is the actual frequency. It can be shown that the clock time error δT after t seconds of operation is

$$\delta T = \frac{\Delta f}{f_o} t \qquad (2.1\text{-}21)$$

This implies that any fixed frequency error $\Delta f/f_o$ will cause a system time error whose absolute value is proportional to time since synchronization.

Long-Term Stability — Crystal clocks exhibit changes in frequency over a period of days. These changes are the result of crystal aging or parametric changes that are partially predictable. Any near-constant rate of change of frequency corresponds to a second derivative of the time error. This results in a quadratic time error build-up.

Short-Term Stability — Short-term stability refers to the effect of small random clock frequency variations over intervals that are short compared to the inverse of the frequency error, $f-f_o$. For the short flight times of tactical missiles this error source may be considered a white noise frequency error which is integrated over the missile flight time to produce a clock phase error.

Error Due to Temperature Variations — The quartz-crystal of the clock is temperature sensitive, and exhibits a frequency shift for a change in temperature. The temperature variations can be assumed to have a spatial distribution. The "thermal mass" of the clock, however, prevents these temperature variations from affecting clock frequency instantaneously. The error due to temperature variations may be considered a white noise frequency error for the short missile flight times of interest and the temperature variations that are likely to be encountered.

Vibration-Induced Errors — Quartz-crystal clocks exhibit a shift in frequency when subjected to random vibrations. This frequency shift depends upon the magnitude and spectrum of the induced vibration. Since the correlation time of the vibration induced error is extremely small, it may be shown (Ref. 1) that for typical measurement rates (Measurements referring to the measurement of propagation time from a master station) this error may be model as a white noise frequency error which is integrated to get clock phase error.

The above-listed error sources may be mathematically represented as (Ref. 1).

$$\delta\varphi_c = \delta\varphi_o + \delta f_o t + \delta_1 t^2 + \int_0^t E(t)\,dt$$

$\delta\varphi_c$ = the total clock phase error in interval t seconds

$\delta\varphi_o$ = initial phase error

δf_o = initial frequency offset

δ_1 = long-term stability coefficient

$E(t)$ = white noise frequency errors due to short-term stability, temperature variations and vibrations.

This equation may be modeled as shown in Fig. 2.1-6.

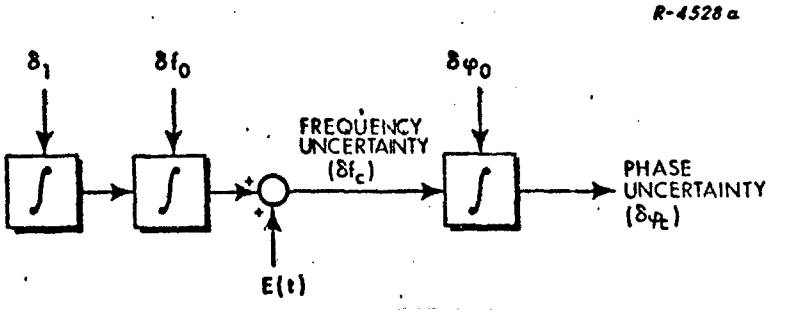

Figure 2.1-6 Clock Error Model

In some modes of operation the clock errors may be calibrated out. The clock error, or clock calibration error if calibration is used, directly effect the error in the range measurement for such systems as Direct Ranging LORAN.

2.1.5 Other External Aid Fix Errors

For some aided inertial guidance techniques (radar correlation, optical correlation, and doppler), the limiting accuracy may be directly related to the fix accuracy of the aiding device. However, errors in the aiding device occur for reasons other than those discussed in the previous sections. The errors in these aiding techniques are dependent on the external aid and will be discussed separately in the sections which cover these guidance techniques.

2.2 LIMITING ACCURACY OF MISSILE GUIDANCE TECHNIQUES

2.2.1 Pure-Inertial Guidance

Pure inertial guidance in tactical missiles refers to the use of an inertial navigator to guide the missile to a precomputed target location.

The accuracy of pure inertial navigation for use in tactical missiles is limited by the errors induced by vertical deflections and gravity anomalies. The rms magnitude of these errors may be computed using Fig. 2.1-5.

To illustrate the use of the figure the following example is presented. Representative values for D_δ and σ_δ are 30 nm and 1.3×10^{-3} ft/sec^2 (8 $\widehat{\text{sec}}$ deflection) respectively. When

$$R = 90 \text{ nm}$$

$$V = 10^3 \text{ ft/sec}$$

Figure 2.1-5 indicates that

$$\sigma_{e_v} \cong 0.47 \text{ ft/sec}$$

$$\sigma_{e_p} \cong 138 \text{ ft}$$

per level loop, at the target.

In the vertical direction, gravity anomalies (variations in the magnitude of gravity) cause navigation errors. These random variations can be modeled in a manner analogous to deflections of the vertical. The vertical position loop of an unaided inertial navigator is unstable. However, the missile flight time is so short that the instability hardly has time to contribute error growth. Considering only the open loop vertical navigation errors, the equations for $\overline{e_v^2}$ and $\overline{e_p^2}$ are the same as those provided above. Only the magnitude of the correlation time T and disturbance standard deviation σ may differ from those of vertical deflections. Representative values of D and σ for gravity anomalies are 30 nm and 3×10^{-5} g's. The resulting rms velocity and position errors in the vertical direction are about 0.35 ft/sec and 103 ft at the end of a 90-nm flight ($V = 10^3$ ft/sec). Thus, the rss velocity and position errors due to vertical deflections and gravity anomalies are 0.75 ft/sec and 220 ft in this example. Errors of this magnitude are not serious when a target homing device is used for terminal guidance systems but serve to illustrate an accuracy limit for pure inertial missile guidance systems if no external position and velocity aids are available. Similar calculations can be carried out for other missile ranges or velocities.

2.2.2 LORAN/Inertial Guidance

Conventional LORAN determines the LOP's on which the receiver lies by measuirng the difference in the time of arrival of signals

from two stations. The LOP's are thus hyperbolic in shape. It is assumed in this analysis that the receiver location measurements provided by LORAN are optimally combined to estimate position errors in the inertial navigator. If many LORAN fixes are taken then all white noise error sources contributing to the LORAN fix accuracy (such as receiver noise) are averaged out. Random bias errors in the LORAN measurements will determine the ultimate limits on accuracy. These bias errors cannot be estimated since the distance of the missile from the LORAN stations is typically large compared to the range of the missile; little geometry change occurs and the bias type errors in the measurements are not observable.

The two major factors which limit the accuracy of a conventional LORAN system are propagation uncertainties, which cause errors in determining the LOP's, and geometric dilution which magnifies radial errors in situations of poor geometry. To illustrate how the equations derived in Section 2.1.1 may be used to determine the accuracy of conventional LORAN an example is presented below.

Assume that a missile is flying in a configuration of LORAN stations as shown in Fig. 2.2-1. As stated previously due to the short flight range of the missile compared to the range to the stations, the geometry may be assumed to be fixed.

Corventional LORAN measures the difference in time of arrival of signals from two stations. LORAN waves are ground waves*

*Skywave propagation becomes important only at large distances from LORAN stations. At these ranges the accuracy greatly decreases so that navigation at large distances from LORAN stations will not be considered.

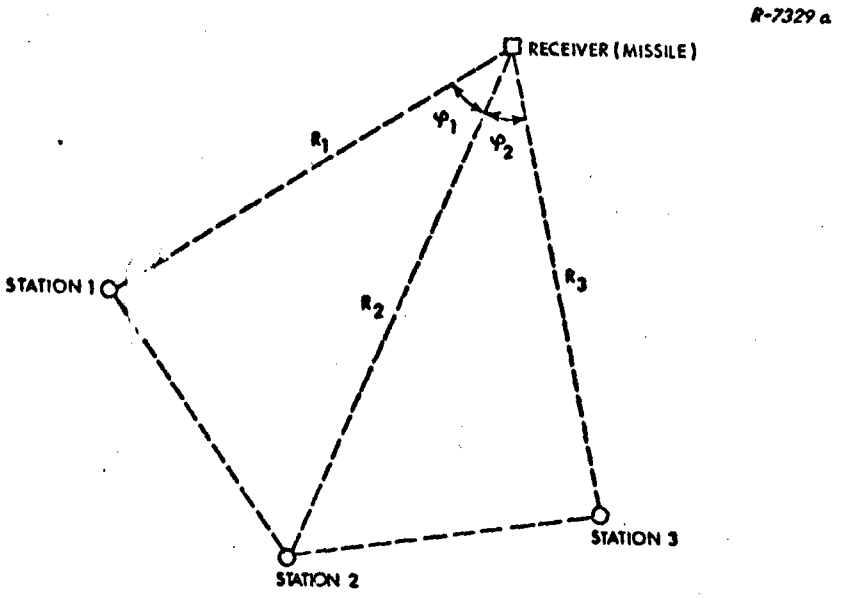

Figure 2.2-1 Configuration of Example Fix Geometry

and the propagation uncertainties are given by Eq. (2.1-14). Using subscrips to denote station numbers, the error in the time difference measurement, ΔT, between stations 1 and 2 and between 2 and 3 are the differences in the propagation uncertainties along the path from each station.

$$\Delta T_{2,1} = \delta T_2 - \delta T_1 = \frac{R_2\alpha_2 - R_1\alpha_1}{c_o}$$

$$\Delta T_{2,3} = \delta T_2 - \delta T_3 = \frac{R_2\alpha_2 - R_3\alpha_3}{c_o} \qquad (2.2\text{-}1)$$

The error in the time difference measurement, ΔT may be viewed as the range from one station being in error by an amount $c_o \Delta T/2$ and the range to the other station by an amount $-c_o \Delta T/2$. Since these range errors are small compared to the range to each station, the indicated LOP can be considered shifted by an amount ϵ as shown in Fig. 2.2-2. From the geometry, the error in determining the LOP is

$$\epsilon = \frac{c_o \Delta T}{2 \sin(\varphi/2)} \qquad (2.2\text{-}2)$$

where φ is the angle between the vectors from the receiver to the stations (see Fig. 2.2-2). Again using subscripts to denote stations, Eqs. (2.2-2) and (2.2-3) can be combined to give

$$\epsilon_{1,2} = \frac{R_2\alpha_2 - R_1\alpha_1}{2 \sin(\varphi_1/2)}$$

$$\epsilon_{2,3} = \frac{R_2\alpha_2 - R_3\alpha_3}{2 \sin(\varphi_2/2)} \qquad (2.2\text{-}3)$$

Squaring these equations and taking the expected value gives

$$\overline{\epsilon_{1,2}^2} = \frac{1}{4 \sin^2\left(\frac{\varphi_1}{2}\right)} \left(R_2^2 \overline{\alpha_2^2} + R_1^2 \overline{\alpha_1^2} - 2R_2R_1 \overline{\alpha_2 \alpha_1}\right)$$

$$\overline{\epsilon_{2,3}^2} = \frac{1}{4 \sin^2\left(\frac{\varphi_2}{2}\right)} \left(R_2^2 \overline{\alpha_2^2} + R_3^2 \overline{\alpha_3^2} - 2R_2R_3 \overline{\alpha_2\alpha_3}\right)$$

$$\overline{\epsilon_{1,2}\epsilon_{2,3}} = \frac{1}{4\sin\left(\frac{\varphi_1}{2}\right)\sin\left(\frac{\varphi_2}{2}\right)}\left(R_2^2\,\overline{\alpha_2^2} - R_1R_2\,\overline{\alpha_1\alpha_2} - R_2R_3\,\overline{\alpha_2\alpha_3} + R_1R_3\,\overline{\alpha_1\alpha_3}\right) \tag{2.2-4}$$

R-7330

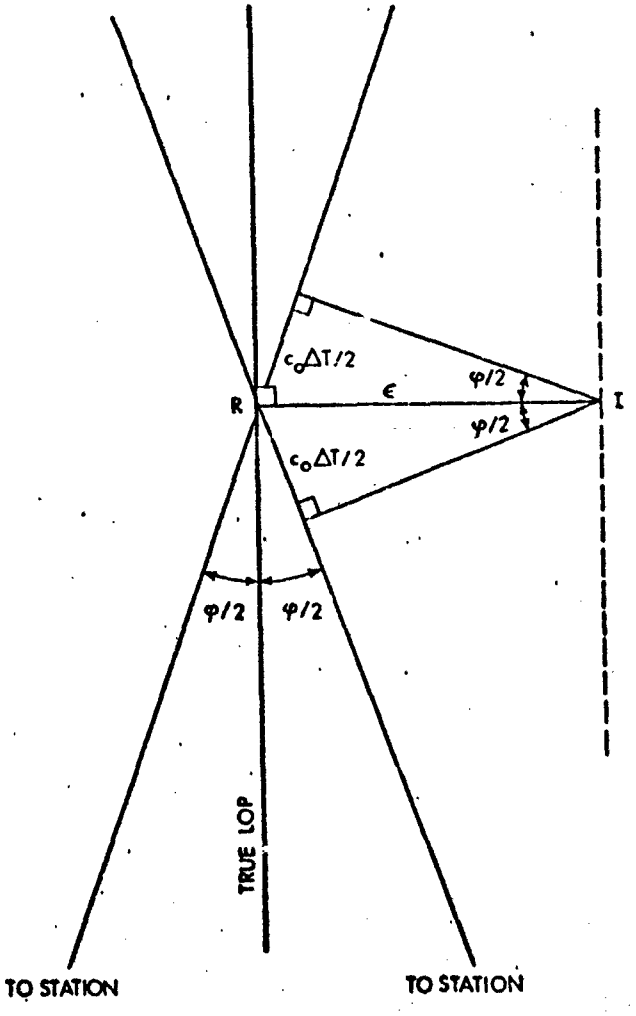

Figure 2.2-2 LOP Error Generated from Error in Propagation Time Difference Measurement from Two Stations

Assuming the LORAN propagation uncertainties from different stations are uncorrelated, Eq. (2.2-4) can be reduced to

$$\sigma_1 = \frac{1}{2\sin\left(\frac{\varphi_1}{2}\right)}\left(R_2^2\,\sigma_{\alpha_2}^2 + R_1^2\,\sigma_{\alpha_1}^2\right)^{1/2}$$

$$\sigma_2 = \frac{1}{2\sin\left(\frac{\varphi_2}{2}\right)}\left(R_2^2\sigma_{\alpha_2}^2 + R_3^2\sigma_{\alpha_3}^2\right)^{1/2}$$

$$\rho = \frac{\overline{\epsilon_{1,2}\,\epsilon_{2,3}}}{\sigma_1\sigma_2}$$

$$= \frac{R_2^2\,\sigma_{\alpha_2}^2}{4\,\sigma_1\sigma_2\sin\left(\frac{\varphi_1}{2}\right)\sin\left(\frac{\varphi_2}{2}\right)} \qquad (2.2\text{-}5)$$

where

σ_1 = standard deviation in the LOP position error from time difference measurement from stations 1 and 2

σ_2 = standard deviation in the LOP position error from time difference measurement from stations 2 and 3

ρ = correlation coefficient between the position errors for the two LOP's

$\sigma_{\alpha_1}, \sigma_{\alpha_2}, \sigma_{\alpha_3}$ = the standard deviations of the propagation scale factor error for each of the three stations

The standard deviation of the radial receiver location error, σ_d, can be found by combining Eqs. (2.2-5) and (2.1-8). To illustrate the use of these equations in solving for the limiting accuracy (radial error) for the LORAN/inertial system the following example is presented: The station geometry shown in Fig. 2.2-3 was assumed. The receiver location was varied about this station configuration and Eq. (2.2-5) was evaluated to determine the standard deviations of the LOP position errors and the correlation coefficient between them. The standard deviation of the radial error was then found from Eq. (2.1-8). These equations were evaluated assuming the propagation uncertainty scale factors, σ_α, have a magnitude of 0.0001. The results are presented in Fig. 2.2-4. This plot provides contour lines of equal radial error. It is interpreted as meaning that the limiting receiver location error (radial) is the value given for the contour line when the receiver lies on that line. Interpolation may be used to determine radial location errors when the receiver lies between contour lines.

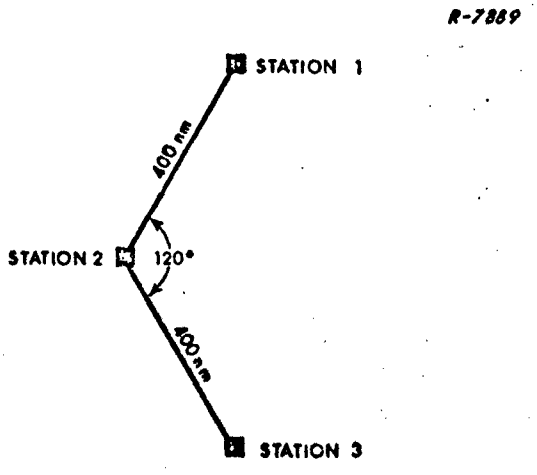

Figure 2.2-3 LORAN Station Geometry Assumed in the Example

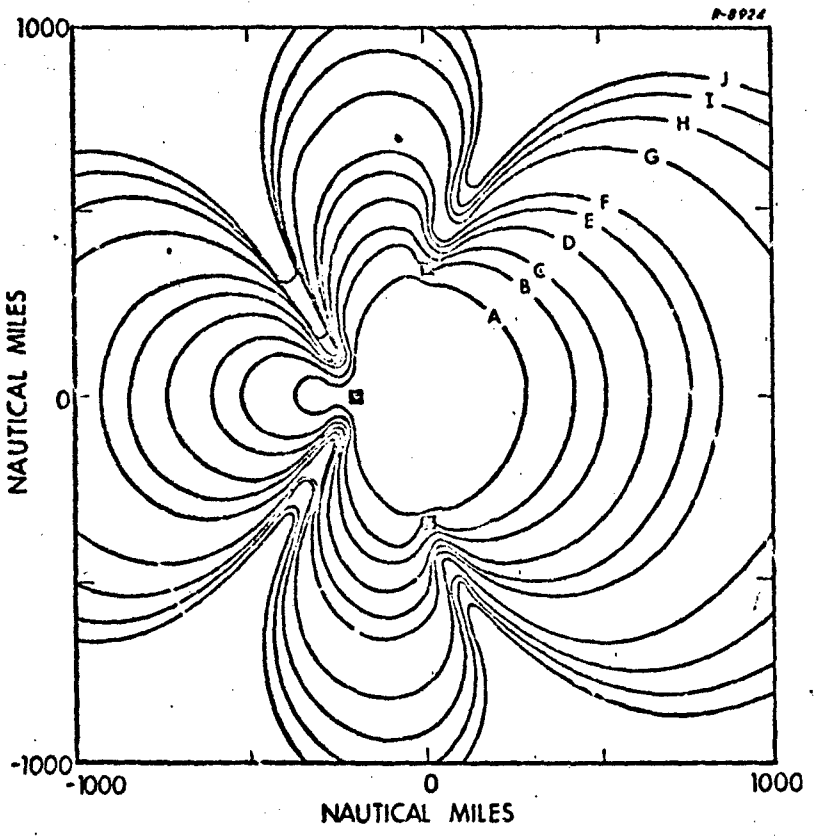

Figure 2.2-4 Limiting Radial Error for LORAN/Inertial Navigation: 10^{-4} Propagation Anomaly

The magnitude of the propagation uncertainty scale factor, σ_α, is dependent on the knowledge of the local propagation variations. It has been established that these may be determined in a given area to the extent that the residual error is given by $\sigma_\alpha = 0.0001$. However without pre-surveying, σ_α may run as high as 0.01. Examination of the equations used to obtain Fig. 2.2-4 shows that the results may be linearly scaled to account for other values of the propagation uncertainty scale factor. For example, if the propagation scale factor is 0.01 the values of the contour levels are simply multiplied by 100.

To illustrate a particular example assume that the missile is located 700 nm from Station 2 and equidistant from Stations 1 and 3 (approximately 600 nm from each). From the figure it may be shown that the limiting accuracy for the LORAN/Inertial system at this location is approximately 2800 ft for a propagation scale factor of 0.0001. This would be acceptable for missile navigation if a homing sensor is used for final guidance to the target. However if there is no knowledge of propagation anomalies and $\sigma_\alpha = 0.01$, the missile location error is 280,000 ft, which is probably unacceptable even with a homing phase. Similar calculations may be carried out to find the radial error for other missile station configurations.

2.2.3 Direct Ranging LORAN/Inertial Guidance

With Direct Ranging LORAN (DRL) the receiver location is determined on a circular LOP by measuring the time required for a signal to travel from a master station. This is accomplished by comparing the time the LORAN signal was sent (information giving the time the signal was sent and the station from which it was sent is contained in the

signal) and the time of signal arrival (determined from an onboard user clock). This time difference can be converted to range from the transmitting station by multiplying the propagation time by the velocity at which radio signals propagate. Measurements from only two stations are required to locate the receiver (assuming an independent measure of altitude), but measurements from three stations are typically used with the redundant information being used to calibrate errors in the user clock and estimate propagation delays. It is assumed in this analysis that the receiver location measurements from three stations are optimally combined to estimate position errors in the inertial navigator, calibrate the user clock, and estimate propagation delays. If many LORAN fixes are taken then all white noise error sources contributing to the LORAN fix accuracy (such as receiver noise) are averaged out. The measurement geometry (the measurement matrix in the Kalman filter formulation) may be assumed fixed since the distance of the missile from the LORAN stations is typically large compared to the range of the missile; little geometry change occurs. It is also assumed that the navigator position errors are very large before the beginning of the processing of LORAN fixes thus making the limiting accuracy of the DRL/inertial system dependent on only the LORAN fix accuracy and not the initial navigator position errors. Since the time of flight of a tactical missile is short the time-varying errors in the inertial system and user clock are ignored.

Since the navigator error dynamics are not considered, the important errors which influence the limiting accuracy of the system are:*

*Notice that this list, together with assumption stated immediately before it, precludes any inertial system error source from having an effect on the limiting accuracy of the DRL/inertial system. The key here is that we are computing limiting accuracy rather than practical accuracy.

x_1 = a navigator position error*

x_2 = b navigator position error*

x_3 = user clock error

x_4 = propagation anomaly scale factor from station 1

x_5 = propagation anomaly scale factor from station 2

x_6 = propagation anomaly scale factor from station 3

We designate $\underline{x}$ as the state vector of these errors

$$\underline{x}^T = \begin{bmatrix} x_1 & x_2 & x_3 & x_4 & x_5 & x_6 \end{bmatrix} \qquad (2.2\text{-}6)$$

and consider P_o to be the initial covariance matrix of these errors before any updates using the LORAN information. The covariance matrix P_n after n sets of updates is given by Eq. (2.2-7).

$$\begin{aligned} P_1^{-1} &= P_o^{-1} + H^T R^{-1} H \\ P_2^{-1} &= P_o^{-1} + 2H^T R^{-1} H \\ &\vdots \\ P_n^{-1} &= P_o^{-1} + nH^T R^{-1} H \end{aligned} \qquad (2.2\text{-}7)$$

*The a, b coordinate frame is any orthogonal set of horizontal coordinates.

where R is the measurement noise matrix for the LORAN fixes and H is the measurement matrix. * By appropriate matrix manipulation Eq. (2.2-7) may be written

$$P_n = P_o - P_o H^T \left(HP_o H^T + R/n\right)^{-1} HP_o \qquad (2.2\text{-}8)$$

As the number of fixes approaches infinity (the limiting case) the equation reduces to

$$P_\infty = P_o - P_o H^T \left(HP_o H^T\right)^{-1} HP_o \qquad (2.2\text{-}9)$$

The covariance of the radial error can then be easily found from the elements of P_∞ as

$$\text{cov (radial error)} = \text{cov}\,(x_1) + \text{cov}\,(x_2) \qquad (2.2\text{-}10)$$

where x_1 and x_2 are defined in the state vector.

For a general three-station configuration as shown in Fig. 2.2-5 the measurement matrix, H, can be defined for the state vector in Eq. (2.2-6) as follows:

$$H = \begin{bmatrix} \frac{(a_r - a_1)}{R_1} & \frac{(b_r - b_1)}{R_1} & 1 & R_1 & 0 & 0 \\ \frac{(a_r - a_2)}{R_2} & \frac{(b_r - b_2)}{R_2} & 1 & 0 & R_2 & 0 \\ \frac{(a_r - a_3)}{R_3} & \frac{(b_r - b_3)}{R_3} & 1 & 0 & 0 & R_3 \end{bmatrix} \qquad (2.2\text{-}11)$$

*This is constant due to the assumption of invariant fix geometry.

where

$$R_1 = \sqrt{(a_r - a_1)^2 + (b_r - b_1)^2}$$

$$R_2 = \sqrt{(a_r - a_2)^2 + (b_r - b_2)^2}$$

$$R_3 = \sqrt{(a_r - a_3)^2 + (b_r - b_3)^2} \qquad (2.2\text{-}12)$$

and the a and b values are defined in the figure.

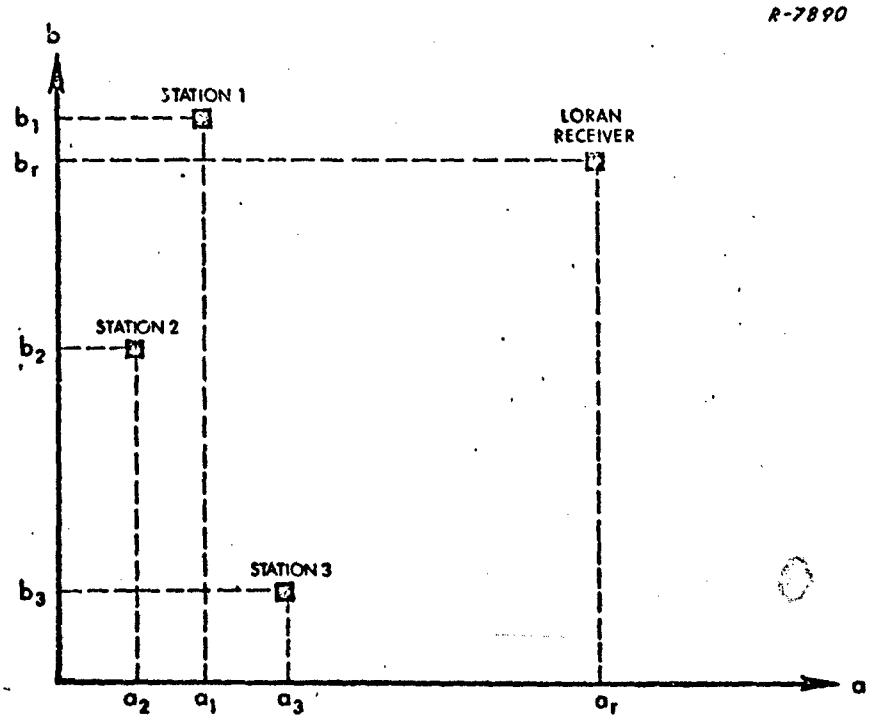

Figure 2.2-5 General Three-Station LORAN Configuration

To illustrate the use of the above method for finding the limiting accuracy (radial error) for the DRL/inertial system the following example is presented: The station geometry shown in Fig. 2.2-3 was assumed. The receiver location was varied about the station configuration and Eq. (2.2-11) was evaluated to determine the measurement matrix, H, at each receiver location. Equation (2.2-9) was solved for each location to determine the covariance of the location errors after an infinite number of fixes. * The covariance of the radial error may then be found from Eq. (2.2-10). Several choices of the initial covariance matrix, P_o, were considered to demonstrate the radial error sensitivity to variations in values of user clock accuracy and propagation anomalies. Table 2.2-1 summarizes the rms values used in the initial covariance matrix for this example and provides the figure number in which the results are plotted. These plots provide contour lines of equal radial error. They may be interpreted in the same manner as the one for the LORAN/inertial system and interpolation may be used between curves.

As stated previously, the initial navigator position errors are assumed to be very large to eliminate the dependence of navigator accuracy from the problem. This is representative of the case in which the navigator has poor prior knowledge of the target location; i.e., only the LORAN grid coordinates of the target are known and the receiver must be located in the LORAN grid.

* As may be seen from Eq. (2.2-8) the actual number of fixes needed to approach this steady-state solution is dependent on the magnitude of the measurement noise matrix, R. For typical systems the number of fixes needed to reach steady state is small and easily achieved under operational conditions.

TABLE 2.2-1

SUMMARY OF INITIAL COVARIANCE VALUES
FOR EXAMPLE RUNS

Initial RMS Value		Figure Number Showing Limiting Accuracy (radial error)
User Clock Error (nsec)	Propagation Anomaly Scale Factor Error*	
300	10^{-4}	2.2-6
500	10^{-4}	2.2-7
300-500	10^{-2}	2.2-8

User clock errors of 300 nsec are considered typical values for quartz-crystal clocks while 500 nsec is considered a worst case (Ref. 1). Therefore, both situations were studied. Also various values for the propagation anomaly scale factor were used since the magnitude is dependent on the knowledge of the local propagation variations. It has been established (Ref. 1) that these may be determined in a given area to the extent that the residual scale factor error is 10^{-4}. However, without presurveying values may run as high as 10^{-2}. Both cases were considered.

Comparison of Figs. 2.2-6 and 2.2-7 shows that the user clock error has its most significant influence on the radial error sensitivity near the LORAN transmitters when propagation anomalies are small. This occurs because when the missile is close to the transmitters the effects of propagation uncertainties are small due to the short distances

*The propagation delays to the receiver from different stations are assumed uncorrelated (Ref. 1).

the radio waves must travel. At large distances the propagation delays become the largest contributor to the radial error, thus decreasing the sensitivity to user clock error.

For large magnitudes of the propagation scale factor error (areas which are not presurveyed) the propagation uncertainties are the dominant error sources contributing to the Direct Ranging LORAN/inertial system. Therefore Fig. 2.2-8 applies for the entire range of user clock errors from 300 to 500 nsec. When the receiver is located near the center of this figure, within the contour line of lowest radial error (50,000 ft), the location accuracy is approximately 50,000 ft. The accuracy does not increase as the receiver moves nearer the transmitting stations since the fix geometry (crossing angles of the LOP's) becomes less favorable in this area for estimation of the propagation delays.

It is interesting to compare the accuracy of the Direct Ranging LORAN/inertial systems with that of hyperbolic LORAN/inertial systems, reported in the previous section. In that section the example chosen assumed the same station configuration as above with the receiver located 700 nm from Station 2 and equidistant from Stations 1 and 3 (approximately 600 nm from each). The results showed that with hyperbolic LORAN/inertial the limiting accuracy at this point was 2,800 ft in presurveyed areas (propagation scale factor = 10^{-4}). From Fig. 2.2-7 it is found that for the worst case user clock accuracy the DRL/inertial radial error is approximately 760 ft. Thus an improvement of at least a factor of 3.6 is achieved with Direct Ranging LORAN. This results from better fix geometry with Direct Ranging LORAN (circular LOP's instead of hyperbolic) and the fact that three measurements are made which are redundant and therefore user clock accuracy and propagation uncertainties may be estimated to a certain extent.

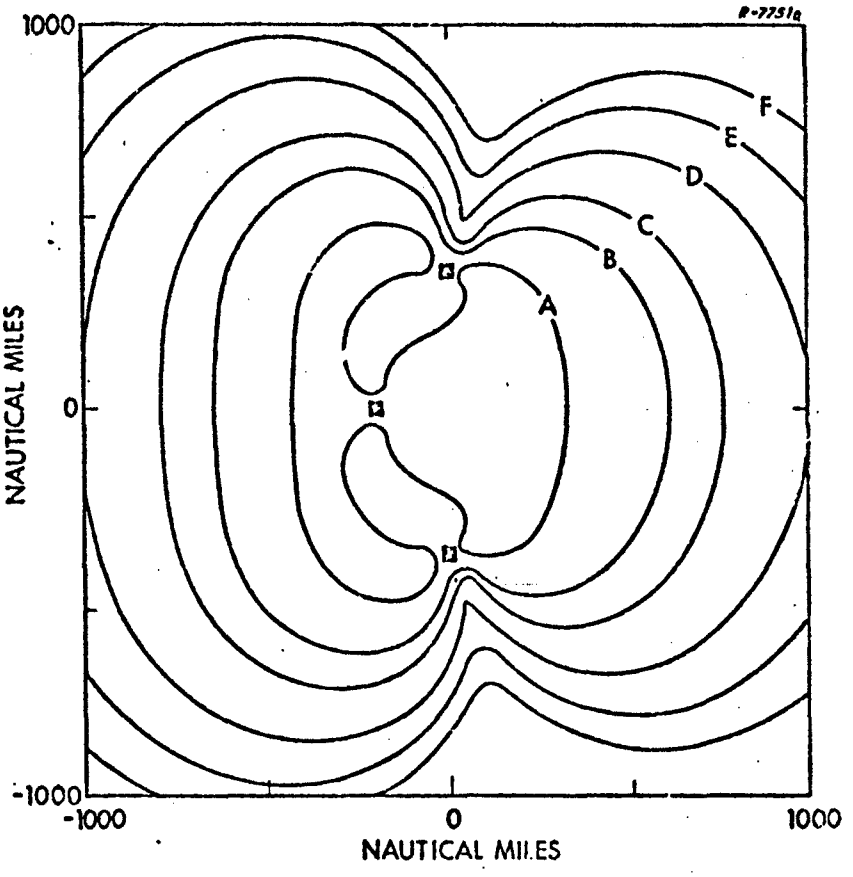

■ TRANSMITTER

USER CLOCK PHASE ERROR = 300 nsec
PROPAGATION ANOMALY SCALE FACTOR = 10^{-4}

RADIAL ERROR
CONTOUR LEVEL VALUES

A = 500 ft	D = 1500 ft
B = 750 ft	E = 2000 ft
C = 1000 ft	F = 2500 ft

Figure 2.2-6 Limiting Radial Error for Direct Ranging LORAN/Inertial Navigation; 300 nsec Clock Error and 10^{-4} Propagation Anomaly

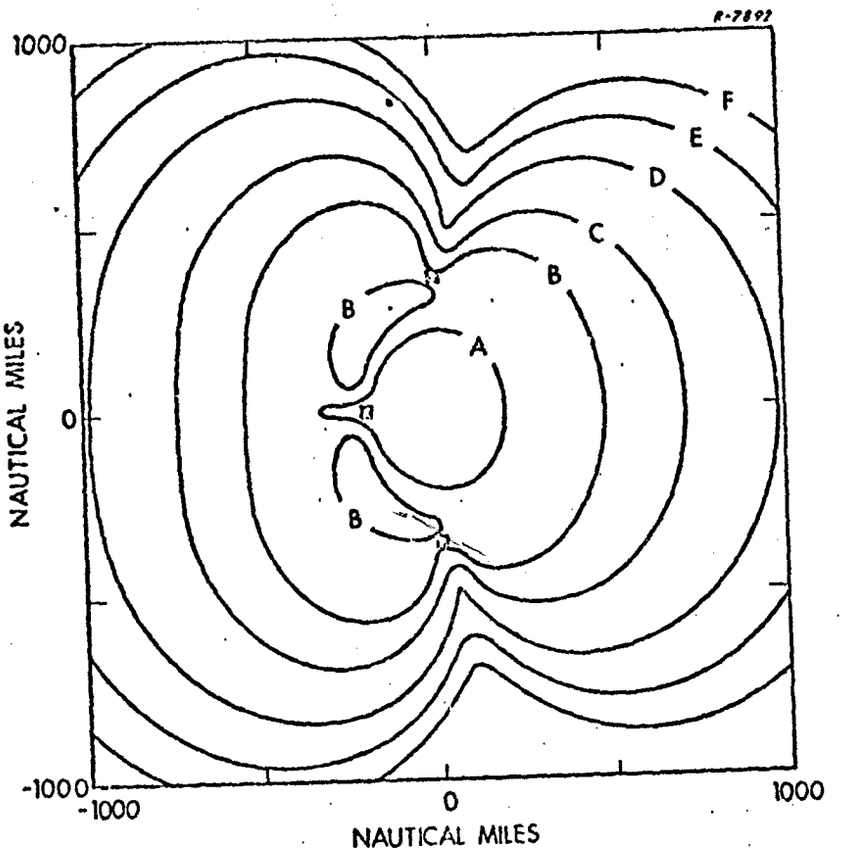

Figure 2.2-7 Limiting Radial Error for Direct Ranging LORAN/Inertial Navigation; 500 nsec Clock Error and 10^{-4} Propagation Anomaly

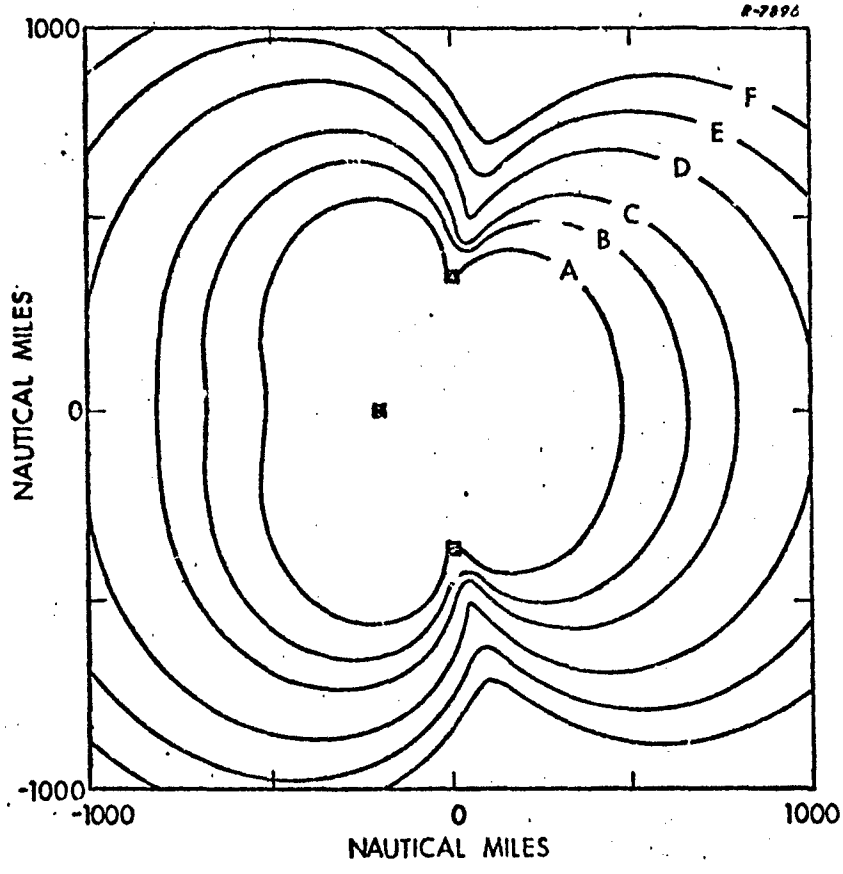

■ TRANSMITTER

USER CLOCK PHASE ERROR = 300 to 500 nsec
PROPAGATION ANOMALY SCALE FACTOR = 10^{-2}

RADIAL ERROR
CONTOUR LEVEL VALUES

A = 50,000 ft	D = 150,000 ft
B = 75,000 ft	E = 200,000 ft
C = 100,000 ft	F = 250,000 ft

Figure 2.2-8 Limiting Radial Error for Direct Ranging LORAN/Inertial Navigation; 300 to 500 nsec Clock Error and 10^{-2} Propagation Anomaly

Examination of Figs. 2.2-6, 2.2-7, and 2.2-8 shows that the DRL/inertial technique provides adequate accuracy for midcourse guidance in presurveyed areas but probably is not acceptable for terminal guidance without additional terminal homing devices. In unsurveyed areas the technique is generally not acceptable.

2.2.4 OMEGA/Inertial Guidance

OMEGA is a long range radio navigation system whose accuracy is limited by propagation uncertainties. OMEGA measures the difference in phase of signals from two stations to locate the receiver on a hyperbolic line of position. The location of the receiver is then the intersection of two LOP's. As with LORAN, the receiver location error is magnified for situations of poor geometry (geometric dilution).

We will assume that the receiver location measurements provided by OMEGA are optimally combined to estimate position errors in the inertial navigator. As with LORAN little geometry change occurs since the range of a tactical missile is typically small compared to the distance of the missile from the stations. For similar reasons as those presented in the previous section it can be shown that the accuracy of the OMEGA/inertial system can be related to the random bias errors in the OMEGA measurements (all white noise error sources may be averaged out by taking many measurements).

OMEGA signals are the skywave type (see Section 2.1.2) and the error in determining a line of position is considered to be a random bias which is uncorrelated with bias errors in LOP determination from other combinations of stations. The present accuracy of OMEGA provides

an error in determining LOP's with a standard deviation of from 0.75 to 1.0 nm (Ref. 4). It is estimated that the theoretical limit on this accuracy is 0.5 nm.

Since the precision of OMEGA is geometry dependent an example will be given to illustrate the calculations necessary to determine the limiting accuracy. For this purpose of this example an OMEGA station configuration as illustrated in Fig. 2.2-9 is assumed. This is representative of the three stations located in Aldra, Norway; Rome, New York; and Trinidad, West Indies. The LOP's are determined by the phase difference of signals from stations 1 and 2 and from stations 2 and 3. Since the measurement errors are uncorrelated and the standard deviation of their magnitudes should be approximately equal, Eq. (2.1-8) can be simplified to give a standard deviation for the radial error as follows:

$$\sigma_d = \frac{\sqrt{2}\,\sigma_m}{\sin\left(\frac{\varphi_1 + \varphi_2}{2}\right)} \qquad (2.2\text{-}13)$$

where σ_m is the standard deviation of the bias errors in the measurement of LOP's and φ_1 and φ_2 are the angles shown in Fig. 2.2-9. The receiver location was varied about the station configuration and Eq. (2.2-13) was evaluated. The limiting accuracy (radial error) for OMEGA/inertial navigation determined in this manner is presented in Fig. 2.2-10 for a 1 nm propagation anomaly bias error. This figure presents contour lines of equal radial error and may be interpreted in the same manner as the one for the LORAN/inertial system. Interpolation may be used between the contour lines. Examination of Eq. (2.2-13) shows that the contour level values may also be linearly scaled to evaluate other values of the propagation anomaly bias error. For example if a

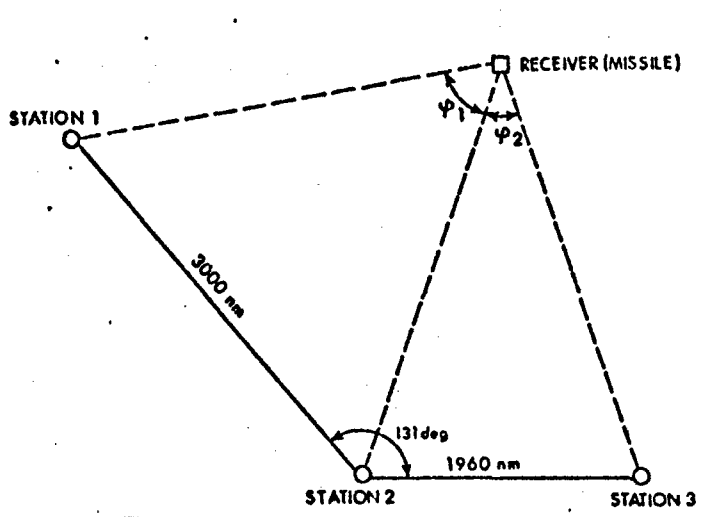

Figure 2.2-9 Configuration of Missile Flight Geometry

propagation anomaly bias error is 0.5 nm the contour level values are multiplied by one-half.

As may be seen from Fig. 2.2-10, over a range of propagation anomaly bias errors from 0.5 to 1.0 nm the accuracy of OMEGA/inertial navigation is probably acceptable for midcourse guidance in areas of good station/receiver geometry. However, a homing sensor for terminal guidance would be needed. Although these results apply to the particular station configuration shown in Fig. 2.2-9, similar calculations can be carried out for other station configurations.

2.2.5 DME/Inertial Guidance

Distance Measuring Equipment (DME) systems are typically short range radio navigation systems which measure range or range and

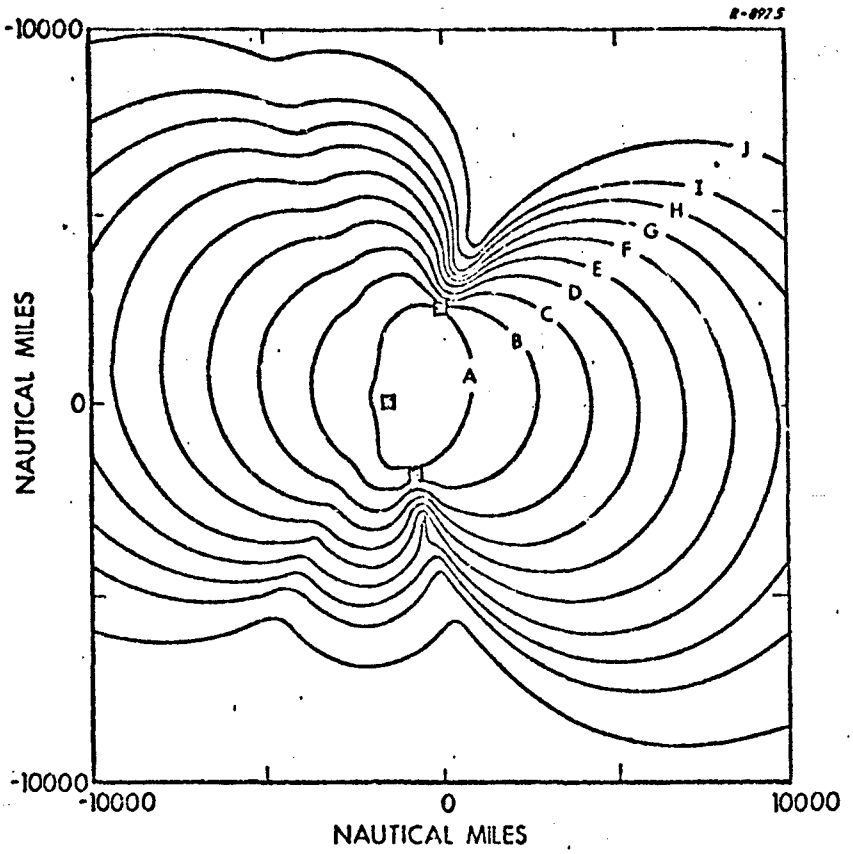

TRANSMITTER

PROPAGATION ANOMALY BIAS ERROR = 1 nm

RADIAL ERROR
CONTOUR LEVEL VALUES

A = 10,000 ft	F = 35,000 ft
B = 15,000 ft	G = 40,000 ft
C = 20,000 ft	H = 45,000 ft
D = 25,000 ft	I = 50,000 ft
E = 30,000 ft	J = 60,000 ft

Figure 2.2-10 Limiting Radial Error for OMEGA/Inertial Navigation; 1 nm Propagation Anomaly Bias Error

velocity of the receiver from one or more transponders. The accuracy of DME systems is a function of the number of transponders, flight path, and sophistication of the data processing techniques used* (number of error sources modeled). Due to the unlimited number of flight paths and station configurations possible, only a qualitative discussion of the accuracy of some particular configurations will be given. Quantitative results would require a separate analysis for each flight configuration.

One Transponder Configuration — A typical one transponder configuration is shown in Fig. 2.2-11. With this configuration, if the relative position between the transponder and missile is approximately known initially by the inertial navigator, as the geometry changes along the flight path the position and velocity of the missile with respect to the transponder can be estimated in the two horizontal dimensions (x and y). To perform this location in the two horizontal dimensions an independent knowledge of altitude are required. For this configuration the horizontal errors in missile location are highly dependent on the altitude error.

By properly taking into account bias or scale factor errors due to propagation uncertainties or other measurement errors in the Kalman type filter used for data processing it is possible to estimate and remove their effects. This occurs since the effect of bias and scale factor errors change with the varying geometry along the flight path.

As stated above a necessary condition for estimating position and velocity is some knowledge of relative position between the transponder and navigator; the navigator position errors become important

*For the discussions which follow optimal data processing is assumed with measurements being incorporated by a Kalman type filter.

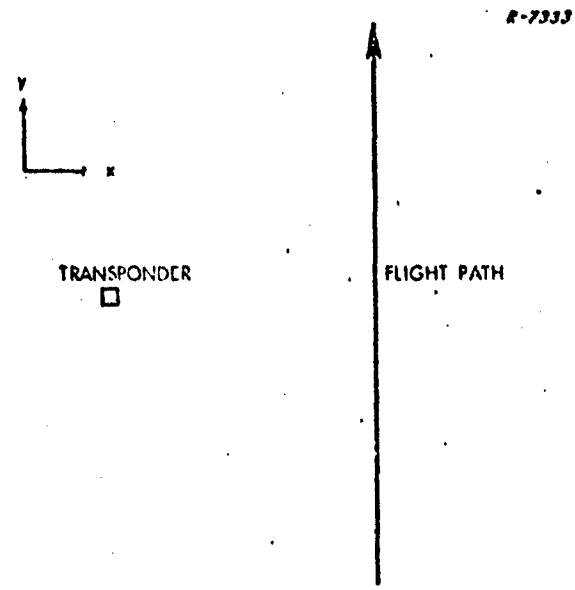

Figure 2.2-11 One-Transponder Flight Configuration

in the ability to resolve the range measurement into two components, x and y. Therefore the navigator position errors enter into the equations used for estimating these very quantities. Typically no difficulty is encountered as long as the position errors are a small fraction of the indicated range to the target. However it is necessary to simulate the system to verify this fact for a particular flight path and initial set of navigator position errors, since the dependence of the measurements on the position errors invalidates normal covariance type analyses (the position errors no longer maintain their zero mean property).

In summary the accuracy of a one transponder DME/inertial system may be said to depend on the following factors:

- Knowledge of the missile altitude.
- Initial knowledge of the relative position between transponder and missile.

- The sophistication of the filter in estimating bias or scale factor errors due to propagation uncertainty and other range or velocity errors.

- Favorability of the flight geometry with respect to the transponder.

Two Transponder Configurations — A representative two transponder configuration is shown in Fig. 2.2-12. Each transponder measures a range to the receiver locating it on a sphere about the transponder. The intersection of the two spheres positions the receiver on a circle. A knowledge of altitude is necessary to determine the receiver location on this circle. Again the altitude error is a significant factor in determining the horizontal location accuracy. The two transponder configuration does eliminate the need for a priori coarse knowledge of relative missile and transponder positions.

As with the single station configuration, by properly modeling bias or scale factor errors in the transponder measurements their effect may be estimated and removed due to geometry changes along the flight path. This would add to the data processing complexity but may allow a significant increase in location accuracy.

The two transponder configuration has an advantage over the one transponder system discussed above in that the additional range measurement (from the second transponder) will both increase the system accuracy and decrease the estimation time of vital parameters (position, velocity, etc.) for most flight configurations. For a further discussion on the evaluation of one particular two transponder DME system refer to Ref. 3.

Three Transponder Configuration — A good three transponder configuration for missile location purposes is shown in Fig. 2.2-13.

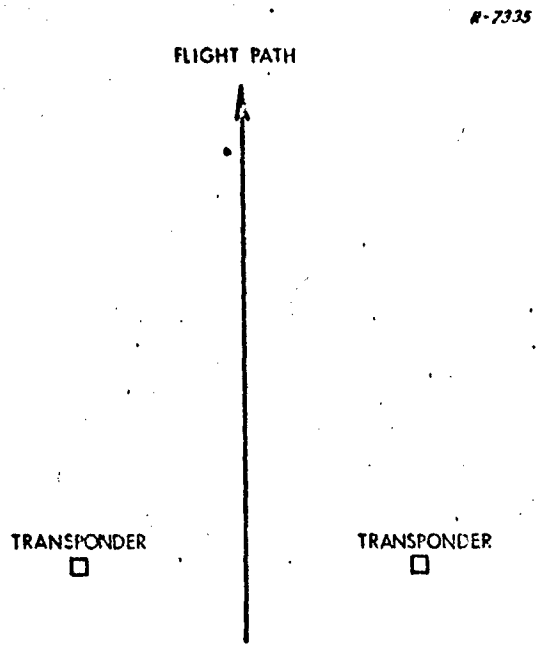

Figure 2.2-12 Two-Transponder Flight Configuration

Since the missile may be located by each transponder on a sphere about itself, the intersection of the three spheres defines the receiver location in three dimensions. Thus receiver location does not depend on external knowledge of missile altitude or prior knowledge of relative location of the navigator and transponders. A flight path passing directly over a transponder as in Fig. 2.2-13 is one of the most desirable for accurate altitude determination. This configuration allows for a measure of altitude as the missile passes directly over the transponder. There may be many three transponder configurations which are unfavorable to altitude determination.

As with the one or two transponder configurations changing geometries along the flight path make it possible to estimate bias or scale factor errors in the measurement if these are properly modeled in the filter.

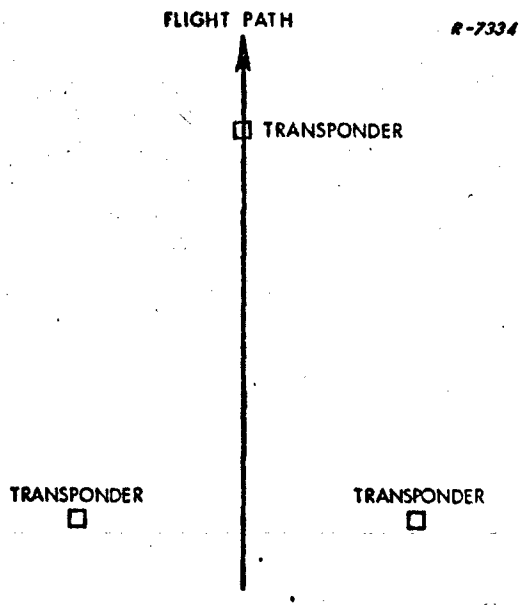

Figure 2.2-13 Three-Transponder Flight Configuration

The addition of the third transponder can provide improved system accuracies and decreased estimation times of vital system parameters. The addition of more transponders over three provides redundant measurements and thus also serves to improve system accuracies.

2.2.6 Satellite/Inertial Guidance

A satellite/inertial system (for example, the synchronous 621B satellite system in Refs. 5 and 6) which determines the receiver location on spheres about each satellite by measuring the time required for a signal to travel from the satellite to the receiver is considered for this analysis. This is accomplished in a manner similar to the Direct Ranging LORAN system discussed previously by comparing the indicated time on a satellite clock at which the signal was sent (information giving the time the signal was sent and the satellite making the transmission is

contained in the signal) and the time of signal arrival (determined from an onboard user clock). This time difference can be converted to range from the transmitting satellite by multiplying the propagation time by the velocity at which radio signals propagate. Errors are introduced into the range measurements due to an uncertainty in the knowledge of the velocity of propagation of the radio waves. Propagation velocity variations result from uncertainties in atmospheric conductivity caused by atmospheric disturbances, water vapor concentration, etc. Measurements from three satellites are required to locate the receiver in three dimensions but a fourth measurement is typically used to calibrate errors in the satellite and user clocks and estimate radio wave propagation uncertainties. Further details and results of the limiting accuracy studies for the satellite/inertial guidance techniques are presented in Volume II (classified SECRET) of this report, Ref. 7.

2.2.7 Radar Correlation/Inertial Guidance

With radar correlation techniques a position fix is made by correlating a predetermined reference map or trace (may be made from reconnaissance or satellite photos) with a "live" return map generated by the missile radar as it flights over the terrain. The location of the reference map is known and when the radar return map matches this reference map the missile position with respect to the reference map is known. Further details and results of the limiting accuracy studies for radar correlation/inertial guidance techniques are presented in Volume II (classified SECRET) of this report, Ref. 7.

2.2.8 Optical Correlation/Inertial Guidance

Optical correlation is similar in principle to radar correlation discussed in the previous section except that optical pictures are matched instead of radar maps. One optical correlation device is the NAFI (Naval Avionics Facility, Indianapolis) Scene Matching Area Correlator (SMAC) which is a passive optical correlation device developed to provide position fixes for a tactical air-to-surface missile. The device correlates a "live" image of the overflown terrain with a stored image obtained by photo reconnaissance. Operation of SMAC is illustrated by Fig. 2.2-14. A reference image of a narrow rectangular strip of land is prepared from aerial reconnaissance photographs. This strip may be as narrow as 2,000 ft. along the direction of flight but its cross-track dimension must be large enough that the missile will be almost certain to fly over some point on the strip. A negative of the reference image is mounted on a rotating drum, the axis of which is usually parallel to the nominal flight path. A live image of the overflown terrain is focused on the moving transparency. As the missile crosses over the strip of land photographed the pre-stored reference image is scanned over the live image by rotating the drum. Since the reference is a negative image and the live scene represents a positive image, there will be a sharp decrease in the amount of light passing through the reference when the two images coincide. This decrease is due to a cancellation of the clear and opaque areas on the stored image with corresponding dark and light area of the live image. Crosstrack position is determined by measuring the distance from one end of the photographic image to the point where match occurs. This is done with the aid of a magnetic pickoff which senses the end-point of the filmed image or the rotating drum. The along track position is established by the fact that the best match occurs when the missile is over the center of the test strip.

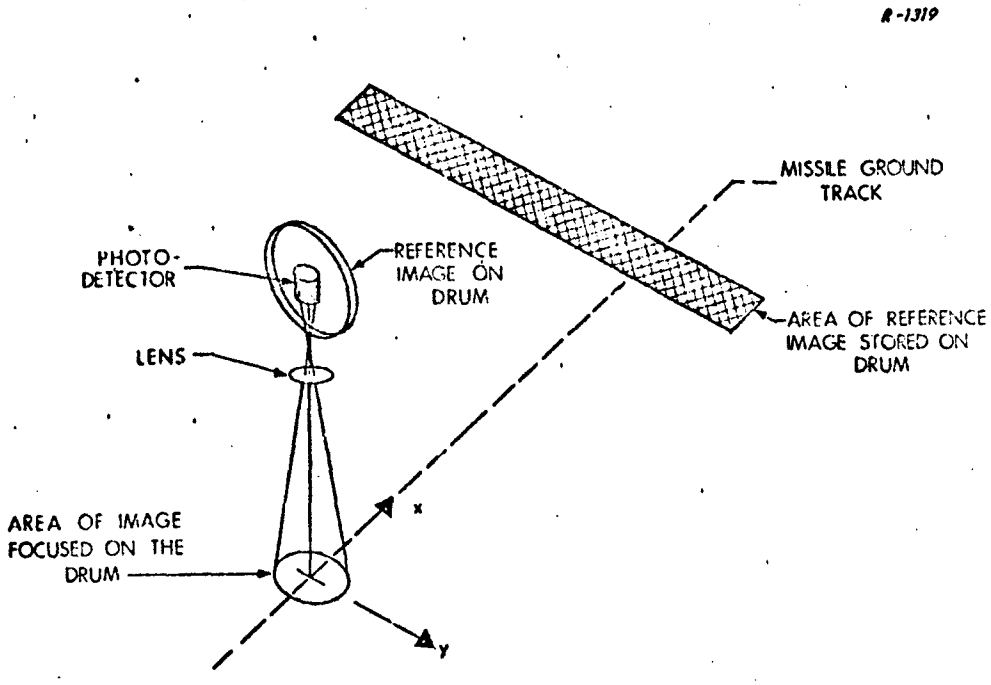

Figure 2.2-14 Scene Matching Area Correlator

Since a reference image must be stored for each fix taken, it is possible to obtain only a few fixes with an optical correlation device. Therefore, the limiting accuracy of an optical correlation/inertial system can be considered to be the position fix accuracy of the optical device.

2.2.9 Doppler/Inertial Guidance

Unlike the other guidance systems discussed in this document, the doppler/inertial system does not provide position updates. It was assumed in the present study that the target location was known without error at the beginning of the flight and therefore the limiting accuracy is simply the position error growth during the flight. The limiting velocity error for the doppler/inertial system is composed of a bias and scale

factor error in the doppler measurement. (Uncorrelated measurement noise can be averaged out if many measurements are taken.) The position error is the integral of the velocity measurement error over the time of flight as expressed by Eq. (2.2-14).

$$\delta P = \int_0^{T_f} \left(\delta V_b + V_m \delta SF\right) dt \qquad (2.2\text{-}14)$$

where

δP = position error
δV_b = bias error in doppler measurement
V_m = missile velocity
δSF = doppler measurement scale factor error
T_f = missile flight time

If the bias and scale factor errors in the doppler measurement are assumed uncorrelated the rms value of the position error becomes

$$\sigma_d = \sqrt{\sigma_{V_b}^2 T_f^2 + \sigma_{SF}^2 \left(\int_o^{T_f} V_m dt\right)^2} \qquad (2.2\text{-}15)$$

where

δ_d = rms position error
δ_{V_b} = rms bias error in doppler measurement
δ_{SF} = rms doppler measurement scale factor error

For example, if the doppler bias error is 0.1 ft/sec, the doppler scale factor error is 10^{-4}, the missile velocity is 2,000 ft/sec, and the missile flies for 200 sec, evaluation of Eq. (2.2-15) indicates an rms value of the limiting position error due to doppler/inertial errors of about 45 ft. As noted previously the determination of the limiting accuracy for the

doppler/inertial system was based on the assumption of perfect knowledge of target location at the beginning of the flight. Since the time of flight of a tactical missile is typically short, correlation between position and velocity errors can be ignored. Therefore, the total delivery error may be considered as the root sum square (rss) of the initial target location error and the position error growth during the flight. *

2.3 CHAPTER SUMMARY

This chapter has presented the analysis of the limiting accuracies for nine aided inertial guidance techniques. The factors shown to limit each technique are summarized in Table 2.3-1. The effects of these factors on each technique are discussed individually in this chapter.

TABLE 2.3-1

FACTORS LIMITING GUIDANCE ACCURACY

	Geophysical Uncertainties	Geometric Dilution	Propagation Uncertainties	Electronic Clock Accuracy	Other External Aid Fix Errors
Pure Inertial	X				
LORAN/Inertial		X	X		
Direct Ranging LORAN/Inertial		X	X	X	
OMEGA/Inertial		X	X		
DME/Inertial		X	X		
Satellite/Inertial		X	X	X	
Radar Correlation/ Inertial					X
Optical Correlation/ Inertial					X
Doppler/Inertial					X

* This technique is valid only if the initial target location error is not dependent on the initial missile velocity error.

3. ACCURACY SENSITIVITY STUDIES FOR AUTONOMOUS MISSILE GUIDANCE

3.1 INTRODUCTION

This chapter discusses the accuracy sensitivity analysis of three inertial guidance techniques for air-to-surface missiles. These guidance techniques are position reference guidance (inertial navigation), heading command guidance, and wind compensated heading command guidance. These analyses relate the sensitivity of missile guidance errors to sensor errors and initial alignment errors for each technique. Five representative trajectories were considered in the analyses. These trajectories were defined to provide typical missile acceleration profiles so that the effect of these accelerations on guidance errors could be studied.

The implementations assumed for the three inertial guidance techniques are as follows:

Position Reference — The inertial navigator considered is representative of a north, east, vertical inertial platform with two accelerometers and three gyros. A vertical channel for the inertial system was not considered. It was assumed that altitude information was derived from a separate source such as a barometric altimeter.

Heading Command Guidance — Heading command guidance is considered to be performed by commanding predetermined missile altitudes and headings with respect to a platform stabilized in inertial space.

(In this analysis altitude information is assumed to be derived from an external source.) The platform is assumed to be gimballed with three gyros mounted on it to provide stabilization. The input axes of these gyros are considered to be mutually orthogonal.

Wind Compensated Heading Command Guidance — Wind compensated heading and altitude command guidance is similar to heading command guidance discussed above. It differs only in that the magnitude of the wind velocity is measured prior to missile launch and this is compensated for throughout the missile flight. The effect of wind on missile accuracy is dependent on the quality of the wind measurement and the spatial variation in magnitude of the wind.

The following sections present a description of the trajectories considered, a discussion of inertial sensor errors, and the results of the analyses of the guidance techniques.

3.2 TRAJECTORIES

Five representative trajectories which might be flown by an air-to-surface missile were considered in the sensitivity analyses. These are discussed separately in the following text.

3.2.1 Cruise-Glide Trajectory

The cruise-glide trajectory is illustrated in Fig. 3.2-1. It consists of a 152 sec straight and level cruise flight at 30,000 ft altitude, followed by a 1-g tip-over maneuver to a pitch angle of -10 deg. The missile then glides at this attitude until it reaches an altitude of 5,000 ft.

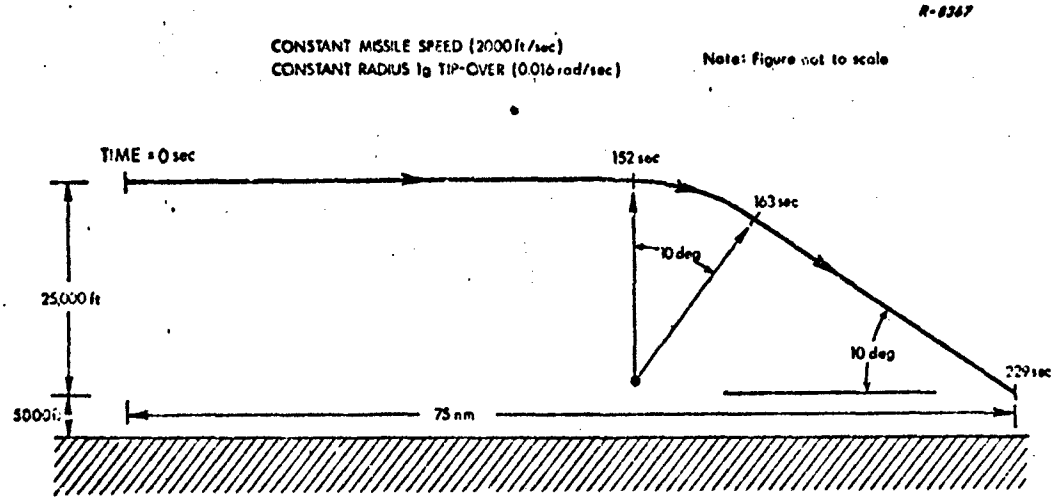

Figure 3.2-1 Cruise-Glide Trajectory

The missile speed is constant (2,000 ft/sec) and it is heading north* during the entire trajectory. Examination of the trajectory shows that the missile accelerates only during the tip-over maneuver. Therefore, acceleration dependent errors are only excited during this maneuver.

3.2.2 Glide-Cruise-Popup Trajectory

The glide-cruise popup trajectory is shown in Fig. 3.2-2. It consists of a 80 sec glide at a pitch angle of -10 deg during which the missile descends from 30,000 ft altitude to about 500 ft. This is followed by a 1-g pull-up maneuver to level and a 78 sec straight and level cruise flight. The missile then performs a popup maneuver in which it does a 4-g pull-up to 45 deg followed by a 2-g tip-over to return the missile to

*The selection of the north heading in this trajectory and others which follow is only for convenience and other headings will not significantly alter the magnitude of the results, only the direction of the errors.

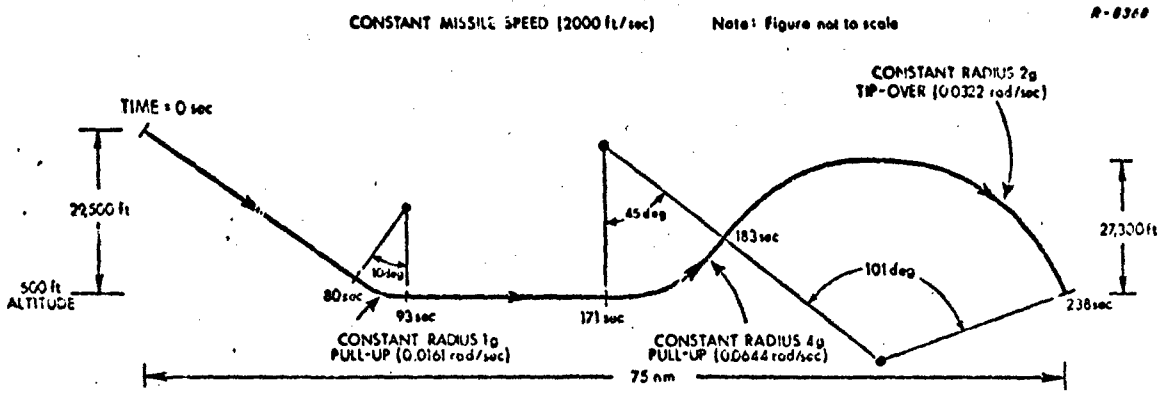

Figure 3.2-2 Glide-Cruise-Popup Trajectory

an altitude of 500 ft. During the tip-over the missile pitch attitude changes 101 deg. The missile speed is constant (2,000 ft/sec) and it is heading north during the entire trajectory. This trajectory contains several high acceleration pull-up and tip-over maneuvers, causing acceleration depend errors to be excited during much of the trajectory.

3.2.3 Loft-Cruise-Glide Trajectory

The loft-cruise-glide trajectory is illustrated in Fig. 3.2-3. It consists of a 5 sec constant acceleration boost phase at a missile pitch angle of 45 deg. During this boost the missile velocity increases from 1,000 ft/sec to 4,000 ft/sec. This is followed by a loft phase during which no missile thrust is applied and the only forces on the missile are due to drag, gravity, and lift. A drag model was chosen in which the dynamic pressure and therefore drag force was proportional to the square of the missile velocity (Ref. 8). Using this model an acceleration profile was obtained which would deliver the missile to an approximate altitude of 25,000 ft with a horizontal velocity of 2,000 ft/sec. The acceleration

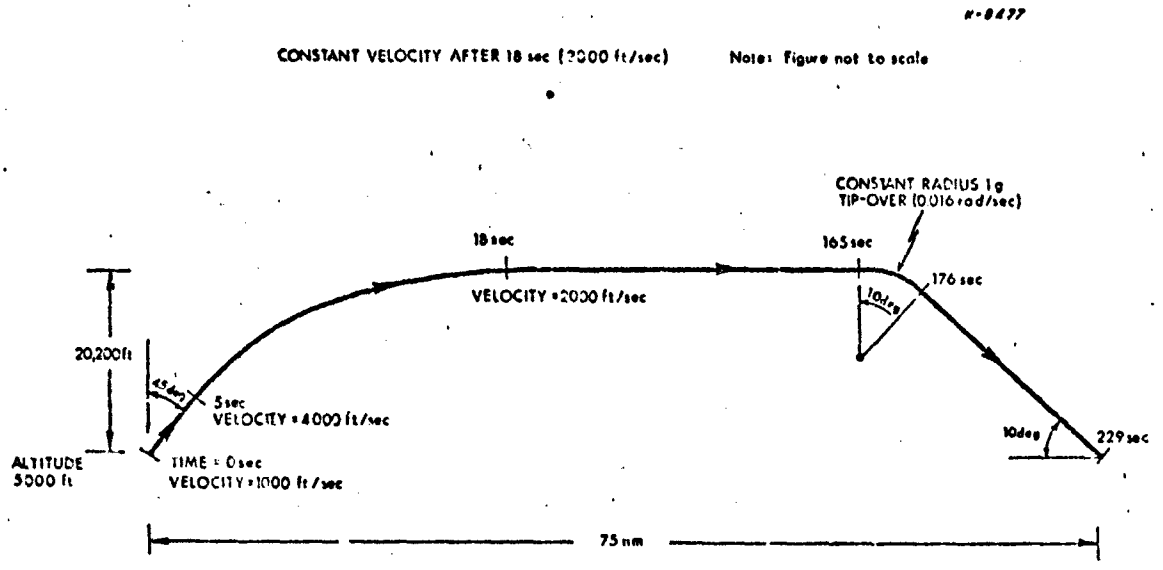

Figure 3.2-3 Loft-Cruise-Glide Trajectory

profile obtained is shown in Fig. 3.2-4. * After the loft phase the missile maintains straight and level flight for 147 sec follow by a 1-g tip-over maneuver to a pitch angle of -10 deg. The missile then glides at this angle to an altitude of 5,000 ft. After the loft phase the missile velocity is constant (2,000 ft/sec) and during the entire trajectory the missile is heading north.

*The actual accelerations experienced by a missile are a function of many parameters such as missile surface area, drag coefficient, guidance law, etc. This profile was chosen since it was felt to be typical of a realistic missile acceleration profile. The purpose of including missile accelerations in this analysis was to provide a realistic representation of the accelerations which excite certain sensor errors. It is felt that other acceleration profiles will excite these sensor errors in a similar manner and that they would cause no significant deviation in the end result.

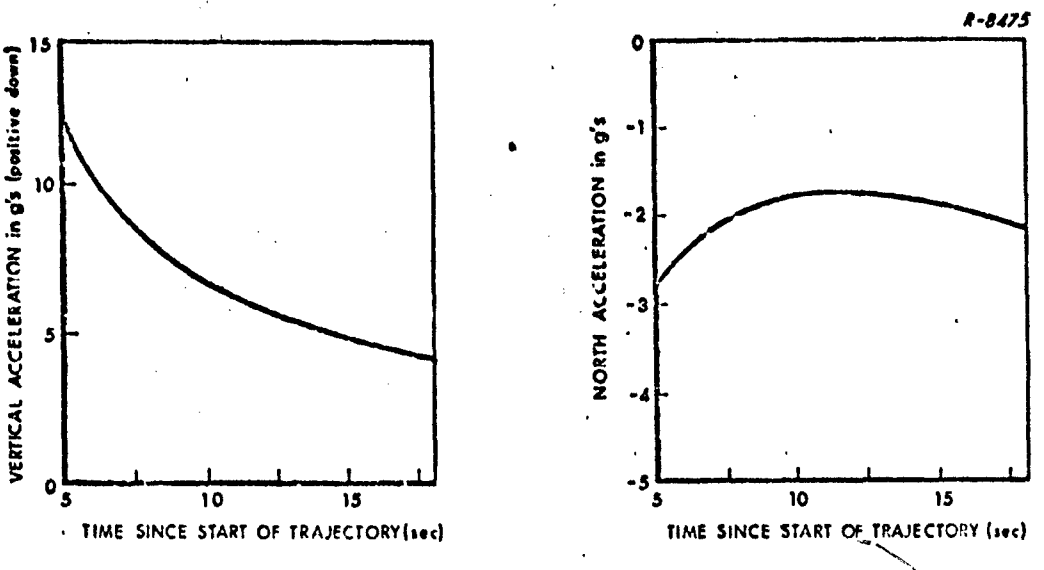

Figure 3.2-4 Acceleration Profile During Loft Phase of Loft-Cruise-Glide Trajectory

3.2.4 Loft-Glide-Cruise Trajectory

The loft-glide-cruise trajectory is illustrated in Fig. 3.2-5. It consists of a boost and loft phase similar to that discussed for the loft-cruise-glide trajectory. This is followed by a 1-g tip-over maneuver to a pitch angle of -10 deg. The missile then glides for 60 seconds and performs a 1-g pull-up to level. It then maintains straight and level flight at an altitude of 500 ft for 129 sec. After the loft phase, the missile velocity is constant (2,000 ft/sec) and during the entire trajectory the missile is heading north.

3.2.5 Turn After Launch With Terminal Popup Trajectory

A trajectory was studied in which the missile performed a turn after launch with a popup maneuver at the end of the trajectory.

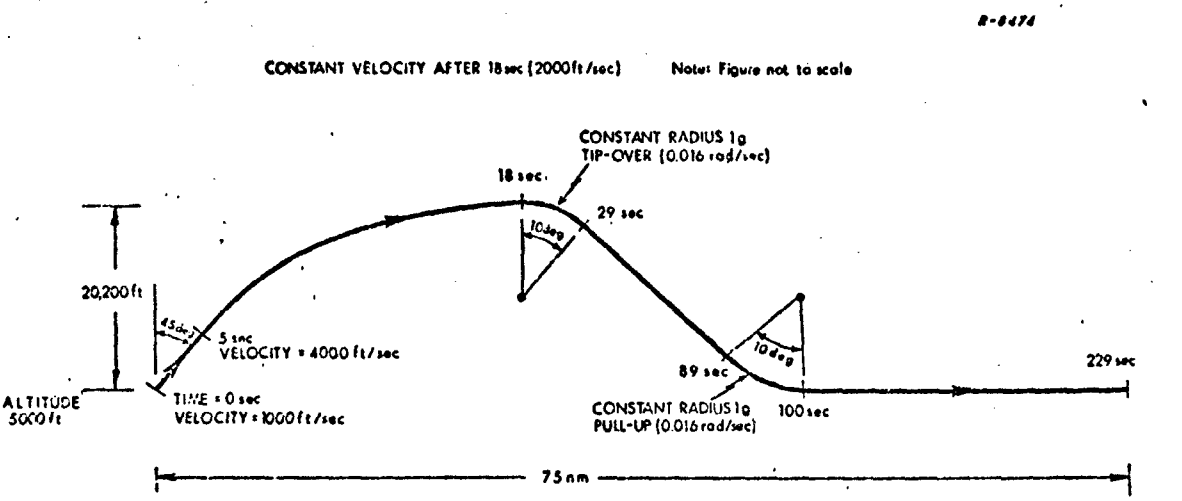

Figure 3.2-5 Loft-Glide-Cruise Trajectory

This trajectory is illustrated in Fig. 3.2-6. The missile is initially heading north but after about 91 sec of straight flight it makes a 1-g 45 deg turn to the left. The terminal popup maneuver was similar to the one discussed in Section 3.2-2 for the glide-cruise-popup trajectory. It consisted of a 4-g pull-up to 45 deg followed by a 2-g tip-over to return the missile to an altitude of 1,000 ft. During the entire trajectory the missile speed was constant (2,000 ft/sec).

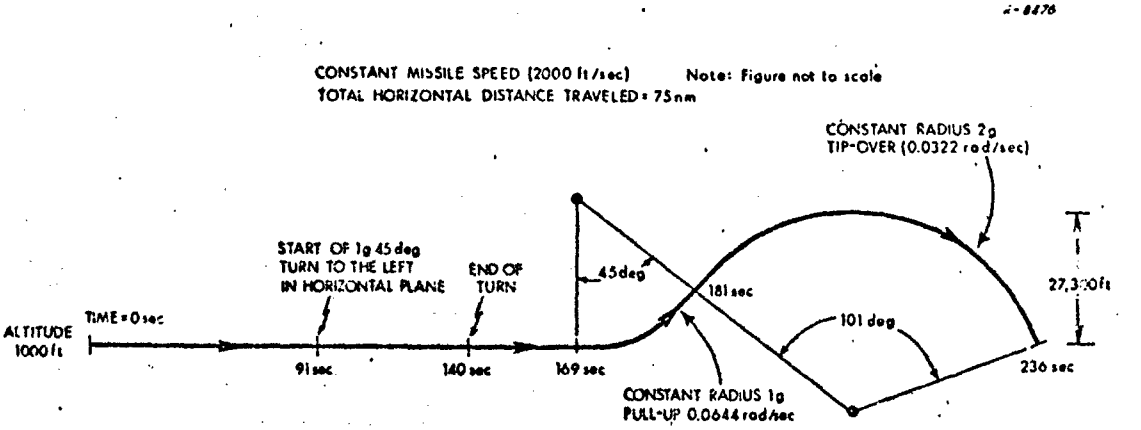

Figure 3.2-6 Vertical Profile of Turn After Launch with Terminal Popup Trajectory

3.3 INERTIAL SENSOR ERRORS

Gyros and accelerometers are not perfect instruments. Errors in these instruments may contribute significantly to position, velocity and attitude errors, especially when missile maneuvers excite the acceleration-sensitive terms. In the sensitivity analyses which were performed, inertial sensor errors were grouped according to type and the effect of each group was then investigated separately. For example, the influence of all the mass unbalance gyro errors was treated as a single effect, rather than investigating mass unbalance errors in the east gyro, etc. What follows is a list of inertial sensor errors considered and an explanation of the grouping used in error sensitivity calculations. The accelerometer errors discussed apply only to position reference guidance since heading command guidance requires only gyros.

Accelerometer Bias Errors — Each of the two inertial navigator accelerometers is considered to have a bias error associated with it. These errors contribute to velocity errors throughout the entire flight.

Accelerometer Scale Factor Errors — These errors generate errors in the sensed acceleration proportional to the specific force components which lie along the instruments' input axes. Errors do not usually appear during unaccelerating flight, but this error source may become significant during high acceleration maneuvers such as turns or a missile boost phase.

Accelerometer Nonlinearities — These imperfections create errors in sensed acceleration that are proportional to the square and

cube of the accelerometer inputs. As with scale factor errors there effects appear during missile maneuvers.

Accelerometer Misalignments — This group consists of two effects due to misalignment of the inertial navigator accelerometer input axes -- one for each of the level accelerometers. In the truth model two accelerometer misalignment terms are omitted because the input axes of the level accelerometers define the navigator platform attitude achieved during alignment. Errors in the sensed acceleration are generated by misresolution of horizontal accelerations through the misalignment angle, causing this effect to appear only during missile manuevers which generate horizontal accelerations.

Gyro Drift Bias Errors — Each of the three gyro input axes* is considered to have a bias drift rate error associated with it. These errors (especially the azimuth gyro drift rate) can cause significant attitude errors. The attitude errors cause misresolution of the specific force vector, generating velocity and position errors.

Gyro Scale Factor Errors — Each gyro input axis is considered to have a drift rate error proportional to the command platform angular rate about that axis. This generally results from imperfect calibration of the gyro torquers. There is one scale factor error term for each of the three gyros in the platform.

Gyro Mass Unbalance Effects — Gyro drift rates proporational to specific force components which lie in the direction of the spin and input axes can be explained in terms of mass unbalance effects. The salient

*Three gyros are assumed on both the inertial navigator and stable platform (used for heading command guidance).

characteristic of this drift rate term is that it is directly proportional to specific force. Since preflight alignment and calibration will permit compensation of the effects of a 1-g environment, mass unbalance drift rate terms will contribute to guidance errors only during missile maneuvers.

Gyro Anisoelasticity Effects — Gyro drift rates proportional to the second power of acceleration result from these effects. Major anisoelastic effects result from simultaneous specific force components along the spin and input axes. They are excited only during missile maneuvers, such as turns and pullups.

3.4 POSITION REFERENCE (INERTIAL) GUIDANCE

The inertial navigator considered in this analysis is representative of a north, east, down inertial platform with two accelerometers and three gyros. A vertical channel for the inertial system is not considered; altitude information is assumed to be derived from a separate source. This section presents the inertial sensor error sensitivity sensitivity tables for the position reference system for the five trajectories discussed previously. The use of the tables provides only the guidance error sensitivity to inertial sensor errors and platform alignment errors. Other sources of error will also be present for the position reference technique, such as the effect of vertical deflections and gravity anomalies on the inertial navigator. These errors have not been explicitly discussed in this section but their influence may be calculated by use of Fig. 2.1-5 in Section 2.1-3.

3.4.1 Inertial Sensor Error Sensitivity Tables

The sensitivity tables for the guidance errors at the end of the five trajectories are presented in this section. Table 3.4-1 presents a summary of the trajectory and corresponding table in which the results may be found. The sensitivity tables give the north and east position and velocity errors along with the CEP of the position errors. These results are given for unit sensor error inputs and in this form are not representative of a particular navigation unit. To use the results the values can be scaled by the proper sensor error value, due to the linearity of the error equations. An example of this scaling is presented in the following section.

TABLE 3.4-1

INDEX FOR SENSITIVITY TABLES

Trajectory	Table Number of Sensitivity Table
Cruise-Glide	3.4-2
Glide-Cruise-Popup	3.4-3
Loft-Cruise-Glide	3.4-4
Loft-Glide-Cruise	3.4-5
Turn After Launch with Terminal Popup	3.4-6

TABLE 3.4-2

SENSITIVITY OF INERTIAL GUIDANCE ERRORS TO SENSOR ERRORS AT THE END OF THE CRUISE-GLIDE TRAJECTORY

Error Source	Unit Sensor Error	North Position Error (ft)	East Position Error (ft)	North Velocity Error (ft/sec)	East Velocity Error (ft/sec)	Position CEP (ft)
Initial position errors	1 ft	9.99×10^{-1}	9.99×10^{-1}	1.66×10^{-5}	1.80×10^{-5}	1.18
Initial velocity errors	1 ft/sec	2.26×10^{2}	2.26×10^{2}	9.60×10^{-1}	9.60×10^{-1}	2.66×10^{2}
Initial tilt errors	1 mr	8.14×10^{2}	8.14×10^{2}	6.93	6.93	9.58×10^{2}
Initial azimuth error	1 mr	3.84	3.82	5.01×10^{-2}	4.70×10^{-2}	3.04
Accelerometer bias errors	1 g	8.39×10^{5}	8.39×10^{5}	7.28×10^{3}	7.28×10^{3}	9.88×10^{5}
Accelerometer bias error correlations with initial tilt errors	0.9	-2.48×10^{4}	-2.48×10^{4}	-2.13×10^{2}	-2.13×10^{2}	-2.92×10^{4}
Accelerometer scale factor errors	1.0	1.93×10^{3}	4.93	2.75×10^{1}	1.41×10^{-1}	1.09×10^{3}
Accelerometer misalignment errors	1 mr	4.93×10^{-3}	1.93	1.41×10^{-4}	2.75×10^{-2}	1.09
Accelerometer nonlinearities (g squared)	$1\ g/g^2$	2.12×10^{2}	5.34×10^{-1}	3.05	1.54×10^{-2}	1.19×10^{2}
Accelerometer nonlinearities (g cubed)	$1\ g/g^3$	2.62×10^{1}	6.54×10^{-2}	3.80×10^{-1}	1.90×10^{-3}	1.47×10^{1}
Gyro drift bias errors	1 deg/hr	2.92×10^{2}	2.92×10^{2}	3.80	3.80	3.44×10^{2}
Gyro drift bias error correlation with initial azimuth error	0.9	-3.18×10^{1}	2.51	-4.14×10^{-1}	3.67×10^{-2}	-1.33×10^{1}
Gyro scale factor errors	1.0	5.77×10^{3}	3.81×10^{3}	7.50×10^{1}	4.96×10^{1}	5.59×10^{3}
Gyro mass unbalance errors	1 (deg/hr)/g	2.97×10^{-1}	3.02×10^{-1}	8.93×10^{-3}	8.92×10^{-3}	3.52×10^{-1}
Gyro anisoelasticity	$1\ (deg/hr)/g^2$	3.11×10^{-6}	1.34×10^{-5}	1.37×10^{-7}	6.04×10^{-6}	7.75×10^{-6}

Minus sign indicates values to be squared and subtracted when rss of error sources is performed to determine the total error

TABLE 3.4-3

SENSITIVITY OF INERTIAL GUIDANCE ERRORS TO SENSOR ERRORS AT THE END OF THE GLIDE-CRUISE-POPUP TRAJECTORY

Error Source	Unit Sensor Error	North Position Error (ft)	East Position Error (ft)	North Velocity Error (ft/sec)	East Velocity Error (ft/sec)	Position CEP (ft)
Initial position errors	1 ft	1.00	1.00	4.05×10^{-5}	3.69×10^{-5}	1.18
Initial velocity errors	1 ft/sec	2.34×10^{2}	2.34×10^{2}	9.57×10^{-1}	9.57×10^{-1}	2.75×10^{2}
Initial tilt errors	1 mr	9.33×10^{2}	9.33×10^{2}	6.70	6.70	1.10×10^{3}
Initial azimuth error	1 mr	4.58	1.42×10^{1}	4.36×10^{-2}	1.37×10^{-1}	8.39
Accelerometer bias errors	1 g	9.01×10^{5}	9.01×10^{5}	7.54×10^{3}	7.54×10^{3}	1.06×10^{6}
Accelerometer bias error correlations with initial tilt errors	0.9	-2.75×10^{4}	-2.75×10^{4}	-2.13×10^{2}	-2.13×10^{2}	-3.24×10^{4}
Accelerometer scale factor errors	1.0	7.51×10^{3}	3.41×10^{1}	2.00×10^{2}	5.46×10^{-1}	4.22×10^{3}
Accelerometer misalignment errors	1 mr	3.41×10^{-2}	7.51	5.45×10^{-4}	2.00×10^{-1}	4.22
Accelerometer nonlinearities (g squared)	$1\ g/g^2$	1.37×10^{4}	2.55×10^{1}	4.60×10^{2}	1.00	7.72×10^{3}
Accelerometer nonlinearities (g cubed)	$1\ g/g^3$	1.32×10^{3}	4.07	9.07×10^{1}	1.18×10^{-1}	9.11×10^{2}
Gyro drift bias errors	1 deg/hr	3.45×10^{2}	3.45×10^{2}	3.25	3.26	4.06×10^{2}
Gyro drift bias error correlation with initial azimuth error	0.9	-3.77×10^{1}	5.44	-3.57×10^{-1}	-6.16×10^{-2}	-1.11×10^{1}
Gyro scale factor errors	1.0	6.73×10^{3}	4.50×10^{3}	6.34×10^{1}	4.25×10^{1}	6.55×10^{3}
Gyro mass unbalance errors	1 (deg/hr)/g	1.69	1.89	1.36×10^{-2}	5.08×10^{-2}	2.10
Gyro anisoelasticity	$1\ (deg/hr)/g^2$	1.00×10^{-2}	1.33×10^{-1}	1.12×10^{-4}	4.60×10^{-3}	7.50×10^{-2}

Minus sign indicates values to be squared and subtracted when rss of error sources is performed to determine the total error

TABLE 3.4-4

SENSITIVITY OF INERTIAL GUIDANCE ERRORS TO SENSOR ERRORS AT THE END OF THE LOFT-CRUISE-GLIDE TRAJECTORY

Error Source	Unit Sensor Error	North Position Error (ft)	East Position Error (ft)	North Velocity Error (ft/sec)	East Velocity Error (ft/sec)	Position CEP (ft)
Initial position errors	1 ft	9.92×10^{-1}	9.83×10^{-1}	5.27×10^{-5}	$8.82\ 10^{-5}$	1.16
Initial velocity errors	1 ft/sec	2.26×10^{2}	2.26×10^{2}	9.60×10^{-1}	9.60×10^{-1}	2.65×10^{2}
Initial tilt errors	1 mr	6.62×10^{2}	6.63×10^{2}	6.16	6.16	7.80×10^{2}
Initial azimuth error	1 mr	6.01	3.00×10^{2}	6.93×10^{-2}	1.20	1.69×10^{2}
Accelerometer bias errors	1 g	8.36×10^{5}	8.36×10^{5}	7.26×10^{3}	7.26×10^{3}	9.84×10^{5}
Accelerometer bias error correlation with initial tilt errors	0.9	-2.23×10^{4}	-2.23×10^{4}	-2.01×10^{2}	-2.01×10^{2}	-2.63×10^{4}
Accelerometer scale factor errors	1.0	2.95×10^{5}	2.49×10^{3}	1.22×10^{3}	2.12×10^{1}	1.66×10^{5}
Accelerometer misalignment errors	1 mr	2.49	2.95×10^{2}	2.12×10^{-2}	1.22	1.66×10^{2}
Accelerometer nonlinearities (g squared)	$1\ g/g^2$	6.60×10^{6}	5.42×10^{4}	2.85×10^{4}	4.74×10^{2}	3.71×10^{6}
Accelerometer nonlinearities (g cubed)	$1\ g/g^3$	8.14×10^{7}	6.71×10^{5}	3.51×10^{5}	5.86×10^{3}	4.58×10^{7}
Gyro drift bias error	1 deg/hr	2.67×10^{2}	2.68×10^{2}	3.65	3.65	3.15×10^{2}
Gyro drift bias error correlation with initial azimuth error	0.9	-3.80×10^{1}	2.10×10^{1}	-4.77×10^{-1}	1.86×10^{-1}	-1.16×10^{1}
Gyro scale factor errors	1.0	5.33×10^{3}	3.49×10^{3}	7.28×10^{1}	4.76×10^{1}	5.14×10^{3}
Gyro mass unbalance errors	1 (deg/hr)/g	7.25×10^{1}	9.93×10^{1}	9.54×10^{-1}	9.67×10^{-1}	9.89×10^{1}
Gyro anisoelasticity	$1\ (deg/hr)/g^2$	1.98×10^{1}	2.01×10^{2}	2.61×10^{-1}	8.67×10^{-1}	1.14×10^{2}

Minus sign indicates values to be squared and subtracted when rss of error sources is performed to determine the total error

TABLE 3.4-5

SENSITIVITY OF INERTIAL GUIDANCE ERRORS TO SENSOR ERRORS AT THE END OF THE LOFT-GLIDE-CRUISE TRAJECTORY

Error Source	Unit Sensor Error	North Position Error (ft)	East Position Error (ft)	North Velocity Error (ft/sec)	East Velocity Error (ft/sec)	Position CEP (ft)
Initial position errors	1 ft	9.92×10^{-1}	9.83×10^{-1}	3.61×10^{-5}	7.23×10^{-5}	1.16
Initial velocity errors	1 ft/sec	2.26×10^{2}	2.26×10^{2}	9.60×10^{-1}	9.60×10^{-1}	2.66×10^{2}
Initial tilt errors	1 mr	6.60×10^{2}	6.60×10^{2}	6.51	6.51	7.76×10^{2}
Initial azimuth error	1 mr	6.40	3.01×10^{2}	7.48×10^{-2}	1.33	1.69×10^{2}
Accelerometer bias errors	1 g	8.37×10^{5}	8.37×10^{5}	7.27×10^{3}	7.27×10^{3}	9.85×10^{5}
Accelerometer bias error correlations with initial tilt errors	0.9	-2.23×10^{4}	-2.23×10^{4}	-2.06×10^{2}	-2.06×10^{2}	-2.62×10^{4}
Accelerometer scale factor errors	1.0	2.95×10^{5}	2.48×10^{3}	1.25×10^{3}	2.12×10^{1}	1.66×10^{5}
Accelerometer misalignment errors	1 mr	2.48	2.95×10^{2}	2.12×10^{-2}	1.25	1.66×10^{2}
Accelerometer nonlinearities (g squared)	$1\ g/g^2$	6.60×10^{6}	5.43×10^{4}	2.85×10^{4}	4.75×10^{2}	3.71×10^{6}
Accelerometer nonlinearities (g cubed)	$1\ g/g^3$	8.15×10^{7}	6.72×10^{5}	3.50×10^{5}	5.86×10^{3}	4.58×10^{7}
Gyro drift bias errors	1 deg/hr	2.98×10^{2}	2.98×10^{2}	4.06	4.06	3.51×10^{2}
Gyro drift bias error correlation with initial azimuth error	0.9	-4.14×10^{1}	2.22×10^{1}	-5.23×10^{-1}	2.00×10^{-1}	-1.24×10^{1}
Gyro scale factor errors	1.0	5.88×10^{3}	3.89×10^{3}	8.05×10^{1}	5.29×10^{1}	5.70×10^{3}
Gyro mass unbalance errors	1 (deg/hr)/g	7.09×10^{1}	9.80×10^{1}	1.03	1.05	9.72×10^{1}
Gyro anisoelasticity	$1\ (deg/hr)/g^2$	2.19×10^{1}	2.07×10^{2}	2.90×10^{-1}	1.08	1.17×10^{2}

Minus sign indicates values to be squared and subtracted when rss of error sources is performed to determine the total error

TABLE 3.4-6

SENSITIVITY OF INERTIAL GUIDANCE ERRORS TO SENSOR ERRORS AT THE END OF THE TRAJECTORY WITH A TURN AFTER LAUNCH AND TERMINAL POPUP

Error Source	Unit Sensor Error	North Position Error (ft)	East Position Error (ft)	North Velocity Error (ft/sec)	East Velocity Error (ft/sec)	Position CEP (ft)
Initial position errors	1 ft	9.99×10^{-1}	1.00	6.95×10^{-5}	3.78×10^{-5}	1.18
Initial velocity errors	1 ft/sec	2.33×10^{2}	2.33×10^{2}	9.57×10^{-1}	9.57×10^{-1}	2.74×10^{2}
Initial tilt errors	1 mr	8.69×10^{2}	8.71×10^{2}	6.31	6.33	1.02×10^{3}
Initial azimuth error	1 mr	1.79×10^{2}	5.68×10^{1}	1.29	6.82×10^{-1}	1.05×10^{2}
Accelerometer bias errors	1 g	8.92×10^{5}	8.92×10^{5}	7.50×10^{3}	7.50×10^{3}	1.05×10^{6}
Accelerometer bias error correlations with initial tilt errors	0.9	-2.64×10^{4}	-2.64×10^{4}	-2.05×10^{2}	-2.07×10^{2}	-3.71×10^{4}
Accelerometer scale factor errors	1.0	6.13×10^{4}	1.74×10^{5}	7.21×10^{2}	1.24×10^{3}	1.36×10^{5}
Accelerometer misalignment errors	1 mr	1.74×10^{2}	6.13×10^{1}	1.24	7.21×10^{-1}	1.36×10^{2}
Accelerometer nonlinearities (g squared)	1 g/g^2	3.58×10^{4}	1.66×10^{5}	4.95×10^{2}	1.51×10^{3}	1.15×10^{5}
Accelerometer nonlinearities (g cubed)	1 g/g^3	1.47×10^{4}	1.49×10^{5}	1.75×10^{2}	1.15×10^{3}	9.27×10^{4}
Gyro drift bias errors	1 deg/hr	3.32×10^{2}	3.20×10^{2}	3.13	3.12	3.64×10^{2}
Gyro drift bias error correlation with initial azimuth error	0.9	-2.26×10^{2}	-1.30×10^{1}	-1.88	-1.55×10^{-1}	-1.22×10^{2}
Gyro scale factor errors	1.0	6.16×10^{3}	4.66×10^{3}	5.81×10^{1}	4.82×10^{1}	6.33×10^{3}
Gyro mass unbalance errors	1 (deg/hr)/g	5.11×10^{1}	4.97×10^{1}	6.26×10^{-1}	6.20×10^{-1}	5.93×10^{1}
Gyro anisoelasticity	1 $(deg/hr)/g^2$	1.42×10^{1}	1.38×10^{1}	1.75×10^{-1}	1.79×10^{-1}	1.65×10^{1}

Minus sign indicates values to be squared and subtracted when rss of error sources is performed to determine the total error

3.4.2 Sample Calculation

The results of the sensitivity analysis can best be used by referring to a particular navigation system. In this section, a typical missile navigation system is described and the guidance accuracies achieved with the previously discussed trajectories are computed. These calculations demonstrate the use of the sensitivity tables and some comparisons which can be made using the results.

A particular alignment scheme and a navigation system which would by typical of a low cost navigator for use in a missile application were assumed. The error coefficients assumed are given in Table 3.4-7.

TABLE 3.4-7

ALIGNMENT AND NAVIGATOR ERRORS

Error Source	Error Magnitude
Initial position errors	200 ft
Initial velocity errors	2 ft/sec
Initial tilt errors	0.1 mr
Initial azimuth error	1.0 mr
Accelerometer bias errors	5×10^{-4} g
Accelerometer bias error correlations with initial tilt error	0.9 correlation coef.
Accelerometer scale factor errors	500 ppm
Accelerometer misalignment errors	1 mr
Accelerometer nonlinearities (g squared)*	8×10^{-5} g/g^2
Accelerometer nonlinearities (g cubed)*	5×10^{-6} g/g^3
Gyro drift bias errors	1 deg/hr
Gyro drift bias error correlations with initial azimuth error	0.9 correlation coef.
Gyro scale factor errors*	1000 ppm
Gyro mass unbalance errors	3.0 deg/hr/g
Gyro anisoelasticity	0.3 deg/hr/g^2

*Values not presently available for LCP III platform, typical values were assumed

Except in the cases noted the sensor performance data for the Raytheon LCP-III low cost inertial platform was used. The alignment scheme to which the numbers correspond might be a transfer alignment from a high quality aircraft navigator with a position update prior to launch.

The guidance error CEP's for the five trajectories, based on the assumed error magnitudes are presented in Table 3.4-8. These were computed by scaling the sensitivity results by the error magnitudes as demonstrated in the following text. Using Table 3.4-2 which contains the sensitivity results for the cruise-glide trajectory, the following calculations can be performed. From the table it can be seen that a 1 ft/sec initial velocity error causes a 226 ft position CEP. The initial velocity error for the alignment scheme assumed was 2 ft/sec (Table 3.4-7). The resultant delivery error CEP is therefore

$$\left[(266 \text{ ft}) / (1 \text{ ft/sec})\right] (2 \text{ ft/sec}) = 532 \text{ ft}$$

All other sensitivity calculations are performed in a similar manner with one exception. When scaling the terms representing correlations between accelerometer bias error and initial tilt error or gyro drift bias error and initial azimuth error the following method must be used: Assume b is the resultant position or velocity error caused by a correlation between error sources x_1 and x_2. If the rms magnitude of x_1 or x_2 or the correlation coefficient for the guidance system being analyzed differs from the unit input value then the result, b, must be scaled as follows. *

*This scaling results since correlation terms are off-diagonal elements in the covariance matrix.

TABLE 3.4-8

CEP OF GUIDANCE POSITION ERRORS FOR 5 TRAJECTORIES

Error Sources	CEP Cruise Glide (ft)	CEP Glide Cruise Popup (ft)	CEP Loft Cruise Glide (ft)	CEP Loft Glide Cruise (ft)	CEP Turn After Launch with Terminal Popup (ft)
Initial position errors	236	236	232	232	236
Initial velocity errors	532	550	530	532	548
Initial tilt errors	96	110	78	78	102
Initial azimuth error	3	9	169	169	105
Accelerometer bias errors	494	530	492	493	525
Accelerometer bias error correlations	-206	-229	-186	-185	-220
Accelerometer scale factor errors	1	2	83	83	68
Accelerometer misalignment errors	1	4	166	166	136
Accelerometer nonlinearities (g squared)	—	1	297	297	9
Accelerometer nonlinearities (g cubed)	—	—	229	229	—
Gyro drift bias errors	344	406	315	351	331
Gyro drift bias error correlations	-13	-11	-12	-12	-122
Gyro scale factor errors	6	7	5	6	6
Gyro mass unbalance errors	1	6	297	292	178
Gyro anisoelasticity	—	—	34	35	5
rss Total	817	873	969	983	890

Minus sign indicates values that were squared and subtracted when rss total was computed

— indicates error sources which had negligible contribution

$$\text{actual rms value} = [b]\sqrt{\frac{\text{rms value of } x_1}{\text{unit input value of } x_1}}\sqrt{\frac{\text{rms value of } x_2}{\text{unit input value of } x_2}}\left[\frac{\text{actual correlation coefficient}}{\text{input correlation coefficient}}\right] \qquad (3.4\text{-}1)$$

To clarify this scaling calculation consider the following example: From Table 3.4-2 for the cruise-glide trajectory, the correction to position CEP caused by a 0.9 correlation between a 1-g accelerometer bias

error and a 1 mr initial tilt error is -2.92×10^4 ft.* For the example considered in Table 3.4-7, the correlation coefficient is 0.9, the accelerometer bias error is 5×10^{-4} g, and the initial tilt error is 0.1 mr. Using the scaling in expression (3.4-1), the resultant correction to position CEP for the example being considered is

$$(-2.92 \times 10^4 \text{ ft})\sqrt{\frac{0.1\text{mr}}{1.0\text{mr}}}\sqrt{\frac{5 \times 10^{-4} \text{ g}}{1\text{g}}}\left(\frac{0.9}{0.9}\right) = -206 \text{ ft}$$

What follows is a partial list of conclusions which can be obtained from these results, to demonstrate their usefulness. It should be noted that the conclusions reached do not apply in general but are dependent on the input values assumed in this example.

- Initial velocity errors are the largest single error contributor for all trajectories. Use of improved initial velocity information (this could be accomplished by doppler aiding the master aircraft navigator before transfer alignment) could significantly reduce this error source. For example if the initial velocity error were reduced to 0.2 ft/sec then the contribution of velocity error would be reduced by a factor of 10 in each case.

- For all trajectories at least 85% of the total rss error was due to initial alignment errors, accelerometer bias error, and gyro drift errors. Improved accuracy could be obtained by improving the alignment scheme and/or using inertial sensors with smaller bias errors.

*The minus sign indicates that the value is to be squared and subtracted when the total rss error is computed. The minus sign shows that the correlation between two error sources helps reduce their total effect.

- In the two trajectories containing a loft phase, the acceleration dependent errors -- accelerometer nonlinearities, gyro mass unbalance, etc. -- generate large guidance errors. Due to the higher contribution of other error sources discussed previously these acceleration dependent errors do not significantly degrade overall performance when compared to trajectories which contain few high accelerations. Therefore, use of improved inertial sensors which have smaller error coefficients for acceleration dependent terms would provide no significant guidance accuracy improvement.

The sensitivity tables presented in this section provide a simple tool for performing accuracy tradeoff studies. They allow the evaluation and comparison of many systems in a short period of time and give insights into areas in which component or procedural changes would be most significant.

3.5 HEADING COMMAND GUIDANCE

This section discusses the sensitivity analysis of the heading command and wind compensated heading command guidance techniques. These techniques differ only in the manner in which wind effects the guidance errors; all other error contributors produce the same guidance errors for the two techniques. Both guidance techniques are considered to be implemented by commanding predetermined missile altitudes and headings with respect to a platform stabilized in inertial space. The platform is assumed to be gimballed with three single-degree-of-freedom gyros mounted on it to provide stabilization as illustrated in Fig. 3.5-1.

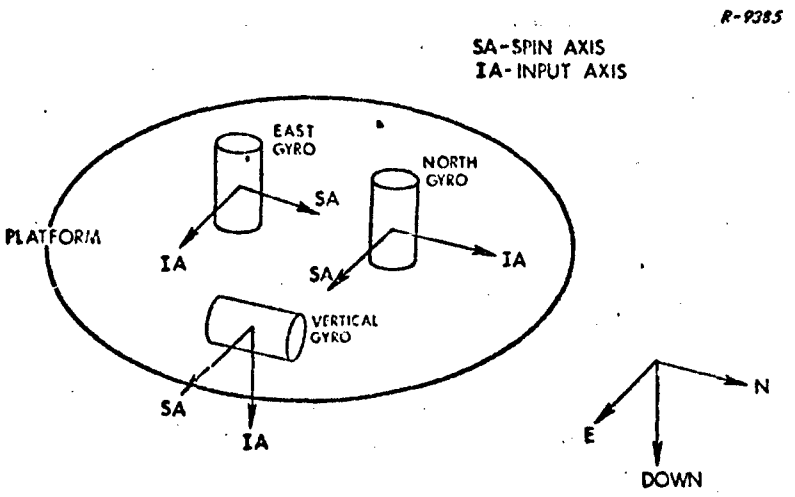

Figure 3.5-1 Gyro Configuration Assumed for Heading Command Guidance

The input axies of these gyros are considered to be mutually orthogonal. * Altitude information is assumed to be derived from an external source.

The inertial sensor error sensitivity tables for the heading command guidance techniques are presented for the five trajectories discussed previously. The use of the tables provides only the guidance error sensitivity to inertial sensor errors and platform alignment errors. Another source of error important for the heading command guidance techniques, the effect of wind, is presented in a separate part of this section. Finally a sample calculation is presented, demonstrating the use of the analyses to evaluate a particular system.

* A second gyro configuration may be used. For this configuration the spin axis of the east gyro is vertical. It was found that this change in configuration does not significantly change the guidance errors for the five trajectories considered.

3.5.1 Inertial Sensor Error Sensitivity Tables

The sensitivity tables for the heading command guidance errors at the end of the five trajectories are presented in this section. Table 3.5-1 presents a summary of the trajectories and corresponding tables in which the results may be found. The sensitivity tables give the along and across track position errors along with the CEP of the position errors.

These results are given for unit sensor error inputs and in this form are not representative of a particular navigation unit. To use the results the values can be scaled by the proper sensor error value (as illustrated in Section 3.4.2), due to the linearity of the error equations.

For convenience, one error contributor which is not attributed to inertial sensors has been included in the sensitivity tables. This error source is the error in the knowledge of the missile velocity and would results from errors in the missile speed indicator or thrust control. For a heading command guidance system which does not rely on external position or velocity information, the along track missile position must be determined from a knowledge of the missile velocity and time of flight. If there is an error in the knowledge of the missile velocity, an error in the along track position will be generated. When external position or velocity information is available, this error will not be significant. In the present analyses the missile velocity error is considered to be directly proportional to the missile velocity.

3.5.2 Wind Compensation

One of the major sources of guidance error when attitude command guidance is used in a cruise missile is the effect of wind. It has

TABLE 3.5-1

INDEX FOR SENSITIVITY TABLES

Trajectory	Table Number
Cruise-Glide	3.5-2
Glide-Cruise-Popup	3.5-3
Loft-Cruise-Glide	3.5-4
Loft-Glide-Cruise	3.5-5
Turn After Launch with Terminal Popup	3.5-6

been suggested that the wind be somehow measured and the commanded heading or velocity be compensated to remove the effects of wind. If a perfect measurement of the wind is achieved and if the wind is constant after the measurement, the influence of wind on guidance errors can be eliminated. In truth the wind is seldom constant and a perfect measurement is not possible. This section analyzes the effect of the wind on missile guidance errors for wind compensated and uncompensated heading command guidance systems when the wind is not constant over the range of the missile. (Temporal variations are ignored in favor of spatial changes in wind velocity.) The wind is further assumed to be a homogeneous, isotropic process allowing the effect of the wind on crosstrack and along track guidance errors to be treated separately.

TABLE 3.5-2

SENSITIVITY OF HEADING COMMAND GUIDANCE ERRORS TO SENSOR ERRORS AT THE END OF THE CRUISE-GLIDE TRAJECTORY

Error Source	Unit Sensor Error	Along Track Position Error (ft)	Across Track Position Error (ft)	Position CEP (ft)
Initial position errors	1 ft	1.0	1.0	1.18
Initial tilt errors	1 mr	2.48×10^{1}	5.96	1.71×10^{1}
Initial azimuth error	1 mr	3.05×10^{-1}	4.56×10^{2}	2.56×10^{2}
Gyro drift bias errors	1 deg/hr	2.33×10^{1}	2.52×10^{2}	1.56×10^{2}
Gyro drift bias error correlation with initial azimuth error	0.9	-2.53	2.23×10^{1}	-1.57
Gyro scale factor errors	1.0	4.58×10^{2}	1.90×10^{3}	1.35×10^{3}
Gyro mass unbalance errors	1 (deg/hr)/g	9.97×10^{-2}	7.42	4.23
Gyro anisoelasticity	1 (deg/hr)/g^2	0	0	0
Velocity scale factor error	1.0	4.56×10^{5}	0	3.10×10^{5}

Minus sign indicates values to be squared and subtracted when rss of error sources is performed to determine the total error

TABLE 3.5-3

SENSITIVITY OF HEADING COMMAND GUIDANCE ERRORS TO SENSOR ERRORS AT THE END OF THE GLIDE-CRUISE-POPUP TRAJECTORY

Error Source	Unit Sensor Error	Along Track Position Error (ft)	Across Track Position Error (ft)	Position CEP (ft)
Initial position errors	1 ft	1.0	1.0	1.18
Initial tilt errors	1 mr	2.73×10^{1}	6.0	1.85×10^{1}
Initial azimuth error	1 mr	1.17×10^{-1}	4.56×10^{2}	2.57×10^{2}
Gyro drift bias errors	1 deg/hr	8.95	2.57×10^{2}	1.50×10^{2}
Gyro drift bias error correlation with initial azimuth	0.9	-9.72×10^{-1}	2.27×10^{1}	1.24
Gyro scale factor errors	1.0	1.67×10^{2}	1.93×10^{3}	1.19×10^{3}
Gyro mass unbalance errors	1 (deg/hr)/g	8.82×10^{-2}	9.78	5.55
Gyro anisoleasticity	1 (deg/hr)/g^2	0	0	0
Velocity scale factor error	1.0	4.56×10^{5}	0	3.10×10^{5}

Minus sign indicates values to be squared and subtracted when rss of error sources is performed to determine the total error

TABLE 3.5-4

SENSITIVITY OF HEADING COMMAND GUIDANCE ERRORS TO SENSOR ERRORS AT THE END OF THE LOFT-CRUISE-GLIDE TRAJECTORY

Error Source	Unit Sensor Error	Along Track Position Error (ft)	Across Track Position Error (ft)	Position CEP (ft)
Initial position errors	1 ft	1.0	1.0	1.18
Initial tilt errors	1 mr	3.9	6.02	5.55
Initial azimuth error	1 mr	2.43×10^{-1}	4.59×10^{2}	2.58×10^{2}
Gyro drift bias errors	1 deg/hr	1.86×10^{1}	2.52×10^{2}	1.53×10^{2}
Gyro drift bias error correlation with initial azimuth error	0.9	-2.02	2.23×10^{1}	-9.40×10^{-1}
Gyro scale factor errors	1.0	3.69×10^{2}	1.89×10^{3}	1.29×10^{3}
Gyro mass unbalance errors	1 (deg/hr)/g	2.11	5.16×10^{1}	3.03×10^{1}
Gyro aniscelasticity	1 (deg/hr)/g^2	0	0	0
Velocity scale factor error	1.0	4.56×10^{5}	0	3.10×10^{5}

Minus sign indicates values to be squared and subtracted when rss of error sources is performed to determine the total error

TABLE 3.5-5

SENSITIVITY OF HEADING COMMAND GUIDANCE ERRORS TO SENSOR ERRORS AT THE END OF THE LOFT-GLIDE-CRUISE TRAJECTORY

Error Source	Unit Sensor Error	Along Track Position Error (ft)	Across Track Position Error (ft)	Position CEP (ft)
Initial position errors	1 ft	1.0	1.0	1.18
Initial tilt errors	1 mr	2.48	6.03	4.71
Initial azimuth error	1 mr	9.27×10^{-2}	4.59×10^{2}	2.58×10^{2}
Gyro drift bias errors	1 deg/hr	7.10	2.53×10^{2}	1.47×10^{2}
Gyro drift bias error correlation with initial azimuth error	0.9	-7.69×10^{-1}	2.24×10^{1}	1.81
Gyro scale factor errors	1.0	1.44×10^{2}	1.90×10^{3}	1.16×10^{3}
Gyro mass unbalance errors	1 (deg/hr)/g	8.78×10^{-1}	5.30×10^{1}	3.03×10^{1}
Gyro anisoelasticity	1 (deg/hr)/g^2	0	0	0
Velocity scale factor error	1.0	4.56×10^{5}	0	3.10×10^{5}

Minus sign indicates values to be squared and subtracted when rss of error sources is performed to determine the total error

TABLE 3.5-6

SENSITIVITY OF HEADING COMMAND GUIDANCE ERRORS TO SENSOR ERRORS AT THE END OF THE TRAJECTORY WITH A TURN AFTER LAUNCH AND TERMINAL POPUP

Error Source	Unit Sensor Error	Along Track Position Error (ft)	Across Track Position Error (ft)	Position CEP (ft)
Initial position errors	1 ft	1.0	1.0	1.18
Initial tilt errors	1 mr	3.83	5.10	4.73
Initial azimuth error	1 mr	1.60×10^{2}	3.96×10^{2}	2.40×10^{2}
Gyro drift bias errors	1 deg/hr	1.34×10^{2}	2.02×10^{2}	1.38×10^{2}
Gyro drift bias error correlation with initial azimuth error	0.9	1.93×10^{1}	7.30×10^{-1}	3.86
Gyro scale factor errors	1.0	1.36×10^{3}	1.88×10^{3}	1.32×10^{3}
Gyro mass unbalance errors	1 (deg/hr)/g	3.26×10^{1}	3.69×10^{1}	2.96×10^{1}
Gyro anisoelasticity	1 (deg/hr)/g^2	3.03×10^{1}	3.45×10^{1}	2.60×10^{1}
Velocity scale factor error	1.0	3.96×10^{5}	1.60×10^{5}	2.40×10^{5}

Minus sign indicates values to be squared and subtracted when rss of error sources is performed to determine the total error

If the wind velocity*, v_w, is represented as a first-order markov process in spatial coordinates, it and the resultant guidance error due to wind, e_w, are related by the following vector-matrix differential equation where T is the characteristic time of the random process.

$$\begin{bmatrix} \dot{v}_w \\ \dot{e}_w \end{bmatrix} = \overbrace{\begin{bmatrix} -\frac{1}{T} & 0 \\ 1 & 0 \end{bmatrix}}^{F} \begin{bmatrix} v_w \\ e_w \end{bmatrix} + \begin{bmatrix} u \\ 0 \end{bmatrix} \qquad (3.5\text{-}1)$$

For a missile with constant velocity**, V, $T = V/D$ where D is the characteristic distance of the wind markov process. The variable u is white noise forcing the first-order linear system whose output is wind:

$$E[u(t)u(\tau)] = \frac{2}{T}\sigma_w^2 \delta(t-\tau)$$

where $\delta(\,)$ is the Dirac delta function and σ_w^2 is the mean square wind velocity.

The covariance equation for the vector

$$\begin{bmatrix} v_w \\ e_w \end{bmatrix}$$

*The derivation which follows is applicable to either an across or along track wind since they may be treated separately.

**The effect of wind on guidance errors is derived for a simplified case of constant missile velocity. The results are still generally applicable for the five trajectories considered in this report since the missile velocity is constant throughout most of these trajectories.

in Eq. (3.5-1) is

$$\dot{P} = FP + PF^T + Q \qquad (3.5\text{-}2)$$

where F is defined in Eq. (3.5-1) and the covariance matrix P is composed of elements

$$p_{11} = E\left(v_w^2\right) \triangleq \sigma_w^2$$

$$p_{12} = E\left(v_w e_w\right)$$

$$p_{22} = E\left(e_w^2\right) \triangleq \sigma_{e_w}^2$$

and

$$Q \triangleq \begin{bmatrix} \frac{2\sigma_w^2}{T} & 0 \\ 0 & 0 \end{bmatrix}$$

From Eq. (3.5-2) the differential equations for the elements of p are

$$\dot{p}_{11} = -\frac{2p_{11}}{T} + \frac{2\sigma_w^2}{T} \quad ; \quad p_{11}(0) = a^2$$

$$\dot{p}_{12} = p_{11} - \frac{p_{12}}{T} \quad ; \quad p_{12}(0) = 0 \qquad (3.5\text{-}3)$$

$$\dot{p}_{22} = 2p_{12} \qquad p_{22}(0) = 0$$

Solving for $p_{22}(t) = \sigma^2_{ew}(t)$, the quantity of interest:

$$\sigma^2_{e_w}(t) = \sigma^2_w T\left[2t - 3T + 4T\,e^{-t/T} - T\,e^{-2t/T}\right] + a^2 T\left[T - 2T\,e^{-t/T} + T\,e^{-2t/T}\right] \tag{3.5-4}$$

Substituting $b \triangleq R/D$ and $T = D/V$ into Eq. (3.5-4) and rearranging we get the relation used to plot Fig. 3.5-2.

$$\sigma^2_{e_w} = \sigma^2_w \left(\frac{R}{V}\right)^2 \frac{1}{b^2}\left[2b - 3 + 4\,e^{-b} - e^{-2b}\right] + a^2\left(\frac{R}{V}\right)^2 \frac{1}{b^2}\left[1 - 2e^{-b} + e^{-2b}\right] \tag{3.5-5}$$

This figure illustrates the important observations that follow from Eq. (3.5-5).

It can be seen that the ratio a/σ_w is an indication of how accurately the wind is measured in a particular situation; when a/σ_w is large a poor measurement of the wind is available. In particular $a/\sigma_w = 1$ corresponds to no measurement of the wind (uncompensated heading command guidance). Figure 3.5-2 indicates that when the missile range is several times the characteristic distance of the wind ($b > 2$) there is little value in having a good measurement of wind. For example, when $b = 2$, σ_{e_w} is only 20% greater when no wind measurement is made

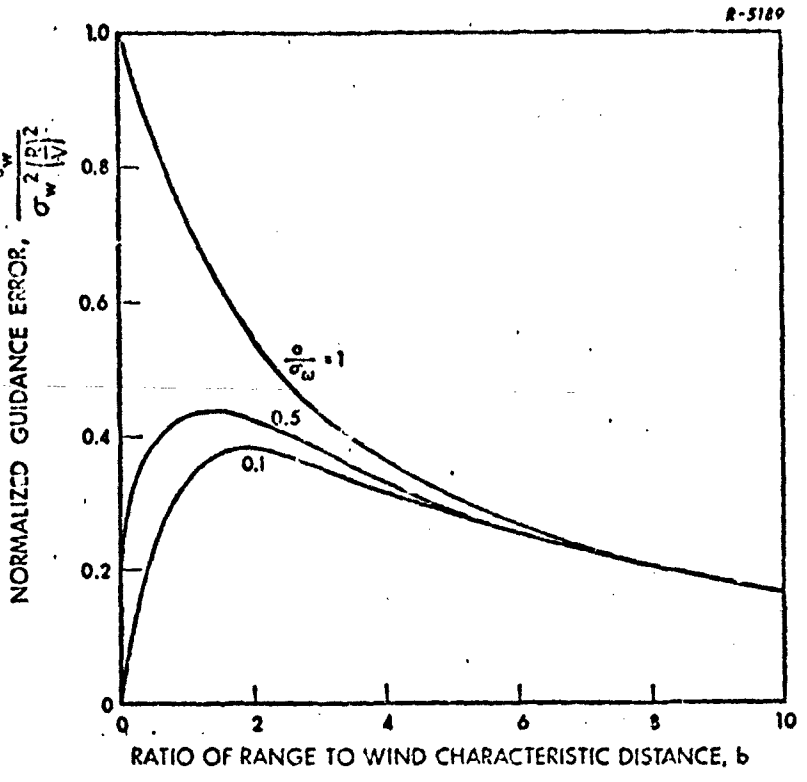

$\sigma_{e_w}^2$ = MEAN SQUARE GUIDANCE ERROR DUE TO WIND

σ_w^2 = MEAN SQUARE WIND

R = RANGE FROM TIME OF WIND MEASUREMENT

V = VELOCITY (ASSUMED CONSTANT)

a^2 = MEAN SQUARE ERROR IN MEASUREMENT OF WIND ($a/\sigma_w = 1$ CORRESPONDS TO NO MEASUREMENT OF WIND)

Figure 3.5-2 **Effect of Wind on Missile Guidance Error for Heading Command Guidance**

than when only 10% error is available. Physically one would expect the value of an initial measurement of wind to diminish as the missile flies through more and more characteristic distances of the first-order markov process which is used here to represent wind. Figure 3.5-1 reinforces this intuitive explanation.

To illustrate the use of Fig. 3.5-2 to calculate the effect of wind on the missile guidance errors the following example is presented: Assume a missile is flying with a 10 ft/sec wind acting on it in the along and across track directions. If the correlation distance of the wind is 150 nm and the missile range is 75 nm (the missile range for all five trajectories discussed in Section 3.2 is 75 nm), the ratio b is 1/2. For the five trajectories studied the velocity is 2000 ft/sec throughout most of the trajectory. Using Fig. 3.5-2, the along track or across track guidance errors can be found based on the above parameters. These are summarized in Table 3.5-7 along with the position CEP. For the particular example chosen the wind correlation distance is sufficiently large with respect to the missile range that significant guidance accuracy improvement can be achieved by wind compensation.

3.5.3 Sample Calculation

As with position reference guidance, the results of the sensitivity analyses can best be used by referring to a particular navigation system. In this section, a typical missile navigation system is described by its assumed error coefficients. The guidance accuracies achieved with the previously discussed trajectories are computed. These calculations demonstrate the use of the sensitivity tables and some comparisons which can be made using the results.

TABLE 3.5-7

EXAMPLE OF THE EFFECT OF WIND
ON GUIDANCE ERRORS

Guidance Technique	Along and Across Track Guidance Error (ft)	Position CEP (ft)
Uncompensated Heading Command Guidance	2100	2480
Wind Compensated Heading Command Guidance with 50% Error in Initial Wind Measurement	1400	1650
Wind Compensated Heading Command Guidance with 10% Error in Initial Wind Measurement	1100	1300

A particular alignment scheme and a stable platform which would be low cost for use in a missile application were assumed. The error coefficients assumed were given in Table 3.5-8. The alignment scheme to which the numbers correspond might be a transfer alignment from a high quality aircraft navigator with a position update prior to launch.

The guidance error CEP's for the five trajectories, based on the assumed error magnitudes are presented in Table 3.5-9. These were computed by scaling the sensitivity results by the error magnitudes, as demonstrated in Section 3.4.2. Table 3.5-9 includes only the effects of alignment and sensor errors and does not include the effect of wind. This effect can be computed separately based on the particular wind parameters, as discussed in the previous section and rss'd to give the total guidance error.

TABLE 3.5-8

ALIGNMENT AND PLATFORM ERRORS

Error Source	Error Magnitude
Initial position errors	200 ft
Initial tilt errors	0.1 mr
Initial azimuth error	1.0 mr
Gyro drift bias errors	1 deg/hr
Gyro drift bias error correlations with initial azimuth error	0.9 correlation coef.
Gyro scale factor errors	1000 ppm
Gyro mass unbalance errors	3.0 deg/hr/g
Gyro anisoelasticity	0.3 deg/hr/g^2
Velocity scale factor error	1000 ppm

What follows is a partial list of conclusions which can be obtained from these results to demonstrate their usefulness. It should be noted that the conclusions reached do not apply in general but are dependent on the input values assumed in this example.

- Gyro errors contribute less than 10% to the total guidance error for all trajectories. Therefore, using more accurate gyros would provide no significant improvement.
- Comparing the results in Table 3.5-9 with the possible effect of wind (discussed in Section 3.5.2), in general it would be expected that wind would cause much larger guidance errors than those contributed by platform sensor and alignment errors.

TABLE 3.5-9

CEP OF GUIDANCE POSITION ERRORS FOR 5 TRAJECTORIES

Error Sources	Cruise Glide (ft)	Glide Cruise Popup (ft)	Loft Cruise Glide (ft)	Loft Glide Cruise (ft)	Turn After Launch with Terminal Popup (ft)
Initial position errors	236	236	236	236	236
Initial tilt errors	2	2	1	—	5
Initial azimuth error	256	257	258	258	240
Gyro drift bias errors	156	150	153	147	138
Gyro drift bias error correlations	-2	1	-1	2	-4
Gyro scale factor errors	1	1	1	1	1
Gyro mass unbalance errors	13	17	91	91	84
Gyro anisoelasticity	0	0	0	0	8
Velocity scale factor error	310	310	310	310	240
TOTAL (rss)	492	490	500	498	444

Minus sign indicates values that were squared and subtracted when rss total was computed.

— indicates error sources which had negligible contribution.

The sensitivity tables in this section provide a simple tool for performing accuracy tradeoff studies. They allow the evaluation and comparison of heading command guidance systems in a short period of time. From them insight can be gained into areas in which component or precedural changes can most significantly reduce guidance errors. The reader is cautioned that when comparing heading command guidance techniques with other guidance techniques, the generally significant contribution of wind must be considered for the particular missile application.

3.6 CHAPTER SUMMARY

This chapter presents the accuracy sensitivity analysis for three inertial guidance techniques; position reference, heading command guidance, and wind compensated heading command guidance. Sensitivity tables are presented for five trajectories relating inertial sensor errors and initial alignment errors to missile guidance errors. Sample calculations are also presented to aid the reader in using the tables. For the heading command guidance techniques, a discussion of wind effects is also presented since this is a potentially significant contributor to guidance errors. No detailed conclusions as to relative accuracy of the techniques can be made since the errors are dependent on the missile and sensor parameters. However, the results in the chapter may be used to achieve detailed comparison of particular systems.

4. SUMMARY

4.1 SUMMARY AND CONCLUSIONS

This report presents the results of two studies dealing with the air-to-surface missile guidance problem. The first portion covers the study of accuracy limits for aided inertial guidance techniques. This involves the computation of the lower bounds on the attainable accuracy of specific guidance techniques. The second part of this document discusses the sensitivity studies which were performed relating missile guidance errors to sensor and alignment errors for three guidance techniques.

The limiting accuracy for nine proposed aided inertial guidance techniques is determined. These systems cover a wide range of possible system designs. The systems studied are:

- Pure Inertial Guidance
- LORAN/Inertial Guidance
- Direct Ranging LORAN/Inertial Guidance
- OMEGA/Inertial Guidance
- DME/Inertial Guidance
- Satellite/Inertial Guidance*
- Radar Correlation/Inertial Guidance*

*Details are presented in Volume II of this report, Ref. 7.

- Optical Correlation/Inertial Guidance
- Doppler/Inertial Guidance

In all cases these systems are assumed to employ an optimum information handling scheme. This assumption provides a consistent baseline against which alternative suboptimal schemes can be compared as well as giving the desired lower limit values.

The accuracy of many of the systems studied was dependent on the missile station geometry. For this reason, the results of the analyses are often presented in the form of contour plots. These plots provide contours of equal guidance error about the station configuration. By this method a large amount of data was conveniently presented for ease of use by the reader.

The second portion of this report presents the sensitivity studies performed for three guidance techniques; pure inertial, heading command, and wind compensated heading command guidance. The results are presented in the form of sensitivity tables which relate the missile guidance errors to inertial sensor and alignment errors for five representative trajectories. These tables allow the rapid evaluation and comparison of inertial sensors and alignment techniques for use in proposed guidance systems. To keep the guidance accuracy assessment in proper perspective, a discussion of another important error source -- the effect of wind -- which is not related to sensor or alignment errors has been included. It is difficult to draw conclusions directly from the sensitivity tables as presented -- they are best used by referring to a particular navigation system. For this reason a sample calculation has been included to demonstrate the use of the tables and some possible conclusions which can be inferred from their use.

4.2 TECHNOLOGICAL FORECAST

This report describes two valuable resources developed for the analysis of missile guidance techniques. The accuracy limit studies for aided inertial guidance techniques provide a lower limit for the spectrum of guidance techniques studied and a consistent baseline against which alternative suboptimal schemes can be compared. These analyses will aid in the evaluation of proposed systems to establish the relative accuracy improvement they may provide. The guidance sensitivity studies are valuable in performing accuracy tradeoff studies of inertial sensors and alignment techniques to establish possible guidance improvements offered by alternative instruments. They also provide an indication of the areas in which component changes will cause the most significant guidance accuracy improvements. These studies provide powerful reference material for use in evaluating proposed guidance systems, both for the present and future. For this reason, summaries of these studies will be incorporated into a future version of the tactical missile guidance handbook, Ref. 9.

REFERENCES

1. Uttam, B. J. and D'Appolito, J. A., "Evaluation of Direct Ranging LORAN Filter Mechanization, Vol. I, Preflight Studies," The Analytic Sciences Corp., AFAL-TR-71-396, February 1972.

2. Sutherland, A. A., Jr., and Bayne, C. D., Jr., "Aided Inertial Guidance for Air-to-Surface Missiles: In-Flight Alignment (U)," Final Report, The Analytic Sciences Corp., TR-145-1, 15 January 1969, CONFIDENTIAL.

3. Sutherland, A. A., Jr., Bayne, C. D., Jr., and Klein, D. W., "Inertial Guidance for Air-to-Surface Missiles: In-Flight Alignment (Continued) (U)," Final Report, The Analytic Sciences Corp., TR-168-1, 15 January 1970, CONFIDENTIAL.

4. Kasper, J. F., Jr., "OMEGA Utilization for Nonmilitary Subscribers, Volume I," The Analytic Sciences Corp., TR-192-2, January 1971.

5. D'Appolito, J. A. and Roy, K. J., "Satellite/Inertial Navigation System Kalman Filter Design Study The Analytic Sciences Corp., AFAL-TR-71-178, June 1971, CONFIDENTIAL.

6. D'Appolito, J. A. and Roy, K. J., "Simulated Satellite/Inertial System Flight Test Support Studies," Final Report, The Analytic Sciences Corp., TR-213-2, October 1971, CONFIDENTIAL.

7. Klein, D. W. and Sutherland, A. A., Jr., "Study of Tactical Missile Guidance: Accuracy Limitations, Vol II (U)," Final Report, The Analytic Sciences Corp., TR-245-1, 28 June 1973, SECRET.

8. Whitehouse, G. D., Caluda, M., and McPhate, A. J., "An Air-to-Surface Missile Simulation Using a Digital Simulation Language," Louisiana State University, Technical Report No. 33, November 1969.

9. Klein, D. W. and Sutherland, A. A., Jr., "Handbook Summary of Midcourse and Terminal Guidance Accuracies," The Analytic Sciences Corp., TIM-245-2, 3 August 1972.

UNCLASSIFIED
Security Classification

DOCUMENT CONTROL DATA - R & D

(Security classification of title, body of abstract and indexing annotation must be entered when the overall report is classified)

1. ORIGINATING ACTIVITY (Corporate author)	2a. REPORT SECURITY CLASSIFICATION
The Analytic Sciences Corporation 6 Jacob Way Reading, Massachusetts 01867	UNCLASSIFIED 2b. GROUP

3. REPORT TITLE

Study of Tactical Missile Guidance: Accuracy Limitations and Guidance Sensitivities, Vol. I

4. DESCRIPTIVE NOTES (Type of report and inclusive dates)

Final Report

5. AUTHOR(S) (First name, middle initial, last name)

Dale W. Klein
Arthur A. Sutherland, Jr.

6. REPORT DATE	7a. TOTAL NO. OF PAGES	7b. NO. OF REFS
June 29, 1973	101	9

8a. CONTRACT OR GRANT NO.	9a. ORIGINATOR'S REPORT NUMBER(S)
N00019-72-C-0392 b. PROJECT NO.	TR-245-1
c.	9b. OTHER REPORT NO(S) (Any other numbers that may be assigned this report)
d.	

10. DISTRIBUTION STATEMENT

1-24-74 TJE

Each transmittal of this document outside agencies of the U. S. Government must have prior approval of the Naval Air Systems Command, AIR-5332.

11. SUPPLEMENTARY NOTES	12. SPONSORING MILITARY ACTIVITY
	Naval Air Systems Command Washington, D. C.

13. ABSTRACT

This report covers the results of limiting guidance accuracy studies for nine proposed aided inertial guidance techniques. In each case an optimum information handling scheme was assumed. This provides a consistent framework for comparing alternative schemes and determining the desired lower limit on errors for each technique. The report also develops the sensitivities of missile guidance errors to sensor errors and initial alignment errors for three unaided guidance techniques -- inertial guidance and heading command guidance with and without wind compensation. The sensitivity tables provided allow rapid comparisons of different inertial sensors and alignment techniques which may be suggested for use in proposed guidance systems.

DISTRIBUTION LIMITED TO U.S. GOVERNMENT AGENCIES ONLY;
- ☐ FOREIGN INFORMATION
- ☐ PROPRIETARY INFORMATION
- ☒ TEST AND EVALUATION
- ☐ CONTRACTOR PERFORMANCE EVALUATION

DATE: 1-24-74
OTHER REQUESTS FOR THIS DOCUMENT MUST BE REFERRED TO COMMANDER, NAVAL AIR SYSTEMS COMMAND, AIR-5332

DD FORM 1 NOV 68 1473 REPLACES DD FORM 1473, 1 JAN 64, WHICH IS OBSOLETE FOR ARMY USE.

UNCLASSIFIED
Security Classification

14. KEY WORDS	LINK A		LINK B		LINK C	
	ROLE	WT	ROLE	WT	ROLE	WT
Aided Inertial Guidance Tactical Missiles Accuracy Limitations Inertial Sensor Sensitivity Analysis						